Cell Reports
Medicine

Article

MYC activation impairs cell-intrinsic IFNγ signaling and confers resistance to anti-PD1/PD-L1 therapy in lung cancer

Graphical abstract

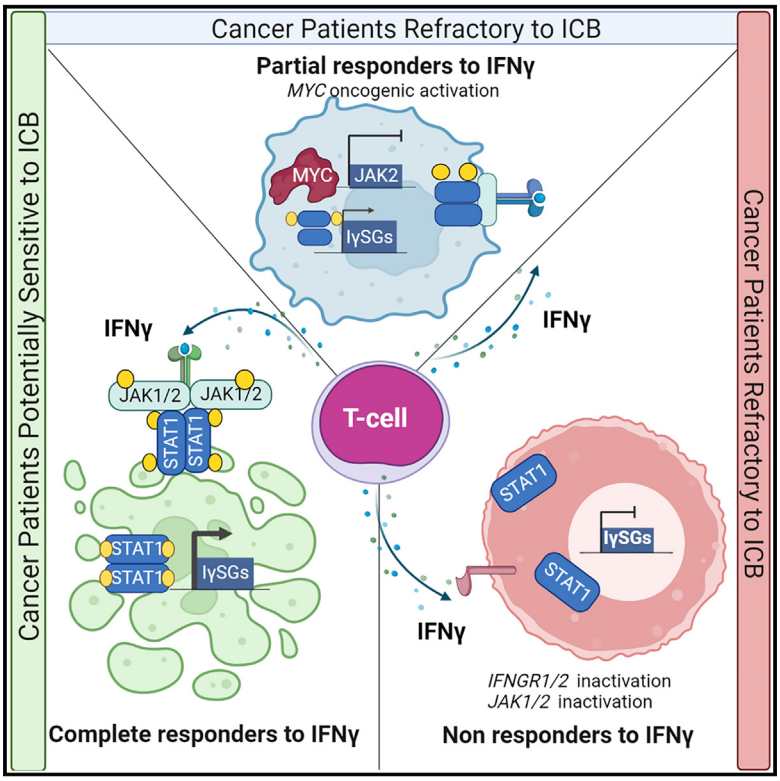

Highlights

- *IFNGR1* inactivation affects a small subset of LCs and prevents the response to IFNγ
- A defective transcriptional activation by IFNγ affects some LCs, preferably SCLCs
- These transcriptional defects are associated with oncogenic *MYC* activation
- *MYC* amplification associates with a worse response to anti-PD1/L1 therapies in LC

Authors

Juan J. Alburquerque-Bejar, Pablo Navajas-Chocarro, Maria Saigi, ..., Manuel Torres-Diz, Anna Esteve-Codina, Montse Sanchez-Cespedes

Correspondence

mscespedes@carrerasresearch.org

In brief

Alburquerque-Bejar et al. show genetic defects that prevent the antitumoral immune response by avoiding the action of IFNγ. One of these impairs IFNγ-mediated transcriptional activation, whereas receptor signaling remains unaffected. Oncogenic MYC is involved in this deficiency. Lung cancer patients with *MYC*-amplified tumors show a poorer response to anti-PD1/PD-L1-based immunotherapies.

Alburquerque-Bejar et al., 2023, Cell Reports Medicine *4*, 101006
April 18, 2023
https://doi.org/10.1016/j.xcrm.2023.101006

CellPress

Cell Reports Medicine

CellPress
OPEN ACCESS

Article

MYC activation impairs cell-intrinsic IFNγ signaling and confers resistance to anti-PD1/PD-L1 therapy in lung cancer

Juan J. Alburquerque-Bejar,[1] Pablo Navajas-Chocarro,[1] Maria Saigi,[2] Ana Ferrero-Andres,[1] Juan M. Morillas,[1] Andrea Vilarrubi,[1] Antonio Gomez,[3] José L. Mate,[4] Ana M. Munoz-Marmol,[4] Octavio A. Romero,[1] Pedro Blecua,[5] Veronica Davalos,[5] Manel Esteller,[5,6,7,8] Eva Pros,[1] Paula Llabata,[1] Manuel Torres-Diz,[1,10] Anna Esteve-Codina,[9] and Montse Sanchez-Cespedes[1,11,12,*]

[1]Cancer Genetics Group, Josep Carreras Leukaemia Research Institute (IJC), IJC Building, Germans Trias i Pujol, Ctra de Can Ruti, Camí de les Escoles s/n, 08916 Badalona, Barcelona, Spain

[2]Department of Medical Oncology, Catalan Institute of Oncology (ICO), Carretera de Canyet, s/n, 08916 Badalona, Barcelona, Spain

[3]Biosciences Department, Faculty of Sciences and Technology (FCT), University of Vic–Central University of Catalonia (UVic-UCC), Carrer de la Sagrada Familia, 7, 08500 Vic, Barcelona, Spain

[4]Pathology Department, Hospital Universitari Germans Trias i Pujol, Carretera de Canyet, s/n, 08916 Badalona, Barcelona, Spain

[5]Cancer Epigenetics Group, Josep Carreras Leukaemia Research Institute (IJC), IJC Building, Germans Trias i Pujol, Ctra de Can Ruti, Cami de les Escoles s/n, 08916 Badalona, Barcelona, Spain

[6]Centro de Investigacion Biomedica en Red Cancer (CIBERONC), Calle Monforte de Lemos, 3-5, Pabellon 11, Planta baja, 28029 Madrid, Spain

[7]Institucio Catalana de Recerca i Estudis Avançats (ICREA), Passeig de Lluis Companys, 23, 08010 Barcelona, Spain

[8]Physiological Sciences Department, School of Medicine and Health Sciences, University of Barcelona, Feixa Llarga, s/n, 08907 l'Hospitalet de Llobregat, Spain

[9]CNAG-CRG, Centre for Genomic Regulation (CRG), Institute of Science and Technology (BIST) and University Pompeu Fabra (UPF), Parc Cientific de Barcelona, Torre I Baldiri Reixac, 4, 08028 Barcelona, Spain

[10]Present address: Division of Cancer Pathobiology, Children's Hospital of Philadelphia, Philadelphia, PA 19104, USA

[11]Twitter: @cespedesmontse

[12]Lead contact

*Correspondence: mscespedes@carrerasresearch.org

https://doi.org/10.1016/j.xcrm.2023.101006

SUMMARY

Elucidating the adaptive mechanisms that prevent host immune response in cancer will help predict efficacy of anti-programmed death-1 (PD1)/L1 therapies. Here, we study the cell-intrinsic response of lung cancer (LC) to interferon-γ (IFNγ), a cytokine that promotes immunoresponse and modulates programmed death-ligand 1 (PD-L1) levels. We report complete refractoriness to IFNγ in a subset of LCs as a result of *JAK2* or *IFNGR1* inactivation. A submaximal response affects another subset that shows constitutive low levels of IFNγ-stimulated genes (IγSGs) coupled with decreased H3K27ac (histone 3 acetylation at lysine 27) deposition and promoter hypermethylation and reduced IFN regulatory factor 1 (IRF1) recruitment to the DNA on IFNγ stimulation. Most of these are neuroendocrine small cell LCs (SCLCs) with oncogenic *MYC/MYCL1/MYCN*. The oncogenic activation of MYC in SCLC cells downregulates JAK2 and impairs IγSGs stimulation by IFNγ. *MYC* amplification tends to associate with a worse response to anti-PD1/L1 therapies. Hence alterations affecting the JAK/STAT pathway and MYC activation prevent stimulation by IFNγ and may predict anti-PD1/L1 efficacy in LC.

INTRODUCTION

To promote their continued survival, cancer cells activate mechanisms that aim to avoid host immune checkpoints and surveillance.[1] Although the precise molecular mechanisms remain poorly understood, in some tumors it involves an increase in the levels of molecules that suppress the activity of the immune system, such as programmed death-1 (PD1) and its ligands PD-L1 and PD-L2.[1] In some cases, this occurs through the activation of oncogenes, such as MET.[2] Therapeutics aiming to boost the immune system have represented a breakthrough in cancer treatment. In most solid tumors, they are based on monoclonal antibodies that block the action of PD-L1 and PD1.[3] These so-called immune checkpoint blockade (ICB) inhibitors show durable antitumor activity in many advanced non-small cell lung cancers (NSCLCs) and so have been enthusiastically incorporated as part of standard care in the treatment of this disease. These therapeutics have not yet been fully implemented, and

other targets and combinatorial treatments are still being investigated.[3–5] Furthermore, reliable biomarkers for patient selection are required. In NSCLC, the levels of PD-L1, tumor mutational burden, and intratumoral CD8 infiltration, among others, have been associated with the response to PD1/PD-L1 blockade.[6] However, most still require validation, and determination of the tumor levels of PD-L1 is currently the only method routinely used in clinical practice.[7] PD-L1 is an imperfect predictor of response, because many tumors with a high level of expression do not respond whereas some tumors with a negative or low level of PD-L1 expression often respond to ICBs.[7]

The tumor's evasion of the host immune system can be triggered by tumor-specific genetic alterations. In addition to the aforementioned genetic activation of MET in lung cancer (LC), which triggers the upregulation of PD-L1 levels,[2] we have previously identified inactivating alterations in the *B2M* and *HLA-A* genes, which are involved in immune recognition, and in *JAK2*, which is involved in the response to interferon-γ (IFNγ), a secreted cytokine that regulates immunity and inflammation.[2,8,9] Immunostaining revealed one-third of lung tumors lack the human leukocyte antigen class I (HLA-I) complex, which is associated with lesser cytotoxic $CD8^+$ lymphocyte infiltration and reduced levels of PD-L1. It also tends to be associated with reduced survival of patients after treatment with ICBs.[8] In contrast, inactivating mutations in *JAK2* in LC cells and in other types of cancer, such as melanoma, prevent the response to IFNγ.[2,10] We also identified a subset of cells that, following stimulation with IFNγ, were able to activate the JAK/STAT pathway but unable to upregulate *CD274*, the gene coding for PD-L1 that is upregulated by IFNγ as part of a feedback inhibition loop ensuring a controlled immunological response.[2] Administering IFNγ triggers the transcriptional activation of genes involved in antigen presentation and the production of chemokines that attract T cells that will ultimately inhibit tumor growth and promote apoptosis.[11–13] Currently, intense efforts are being devoted to determining the influence of the tumor immune microenvironment on predicting host immune response and sensitivity to ICB.[14]

Given that the ability to properly activate IFNγ signaling has been implicated in the efficacy of ICBs treatments[10,13] and that the intrinsic characteristics of the tumor decisively modulate the composition of the tumor microenvironment, we decided to dissect the mechanisms that impair the cell-autonomous response to IFNγ in LC.

RESULTS

Deficiencies in the cell-intrinsic response to IFNγ among LC cells

IFNγ binds a specific cell-surface receptor complex, a heterodimer of IFNGR1 and IFNGR2, expressed in most cell types, which employ JAK1 and JAK2 to phosphorylate STAT1 (pSTAT1). pSTAT1 homodimers translocate to the nucleus and stimulate the expression of a set of genes, including transcription factors such as IFN regulatory factor 1, *IRF1*, by binding to gamma IFN-activated sites (GASs).[11,12] To characterize the response to IFNγ in a panel of human LC cell lines and patient-derived cancer cells (PDCs),[15] we measured the activation of JAK/STAT signaling and the transcriptional activation of IFNγ-stimulated genes (IγSGs), including *CD274*, the gene that codes for PD-L1 (Figures 1A and 1B). On administration of IFNγ, we distinguished three different types of response among the LC cells (Figure 1C): (1) showed activation of the signal transduction molecules (phosphorylation at STAT1 and increase of IRF1), as well as transactivation of six IγSGs tested (complete responders [comp-Rs]); (2) showed activation of STAT1 and IRF1, but not (or minimal) transactivation of the IγSGs (Figure 1B), including PD-L1 (partial responders [part-Rs]); and (3) showed no activation of STAT1 and IRF1 or transcriptional activation of IγSGs (non-Rs). Considering the various LC cells, the proportions of non-R, part-R, and comp-R were 6% (n = 4), 38% (n = 25), and 56% (n = 37), respectively. The part-R group was significantly overrepresented in small-cell LCs (SCLCs) (Figure 1D). The *JAK2*-mutant cells (H1573, H1993, and H2126), as we previously reported, were included in the non-R cell type.[2] Alterations of genes involved in immunorecognition, such as *B2M*, did not affect the intrinsic response to IFNγ (Table S1).

IFNα also plays an important role in tumor immune surveillance and affects tumor cell growth and proliferation, among other functions.[17] To determine whether the defects in the response to IFNγ in the part-R cells also affect that of IFNα, we administered IFNα to a small subset of non-R, part-R, and comp-R cells. On IFNα administration, all LC cells showed an increase of pSTAT1 levels and of different transcripts that are specific targets of IFNα (Figure S1). IFNα administration did not trigger upregulation of PD-L1 or IRF1 in any of the LC cells tested. These data support that the deficient response to IFNγ in the part-R and non-R cells does not affect response to IFNα.

IFNγ-mediated signaling impaired by genetic inactivation of IFNγ receptor 1 in LC

According to our whole-exome sequencing data, the PDC11 cells feature a tumor-specific biallelic inactivation of the IFNγ receptor 1 gene, *IFNGR1*.[15] Here, we confirmed the presence of this alteration and the lack of IFNGR1 protein (Figures 2A and 2B). Germline loss-of-function mutations in *IFNGR1* lead to immunodeficiencies and malignancies.[18] Further, somatic inactivation of *IFNGR1* has been reported in melanoma.[10] The frequency of inactivation of *IFNGR1* reported in databases for human cancer is less than 1%. We analyzed data from the Cancer Cell Line Encyclopedia (CCLE) (961 cancer cell lines of most tumor types) and from The Cancer Genome Atlas (TCGA) (1,144 pan-lung primary tumors), at cBioPortal, to determine the frequency of putative loss-of-function mutations in *IFNGR1*. Five (0.5%) and three (0.3%) truncating mutations were identified in each cohort, respectively (Figure S2A). We also used Sanger direct sequencing to determine the frequency of mutations in a cohort of treatment-naive stage I–III lung primary tumors (n = 88) and collected data from 39 lung tumors (primary tumors, patient-derived xenografts, and patient-derived cancer cells) from whole-exome sequencing studies.[8,15] The screening identified different changes at *IFNGR1* of unknown significance and some single-nucleotide polymorphisms (Table S2).

We noticed that, in contrast with the *JAK2*-mutant, the *IFNGR1*-mutant cells show extremely high levels of PD-L1 protein

CellPress
OPEN ACCESS

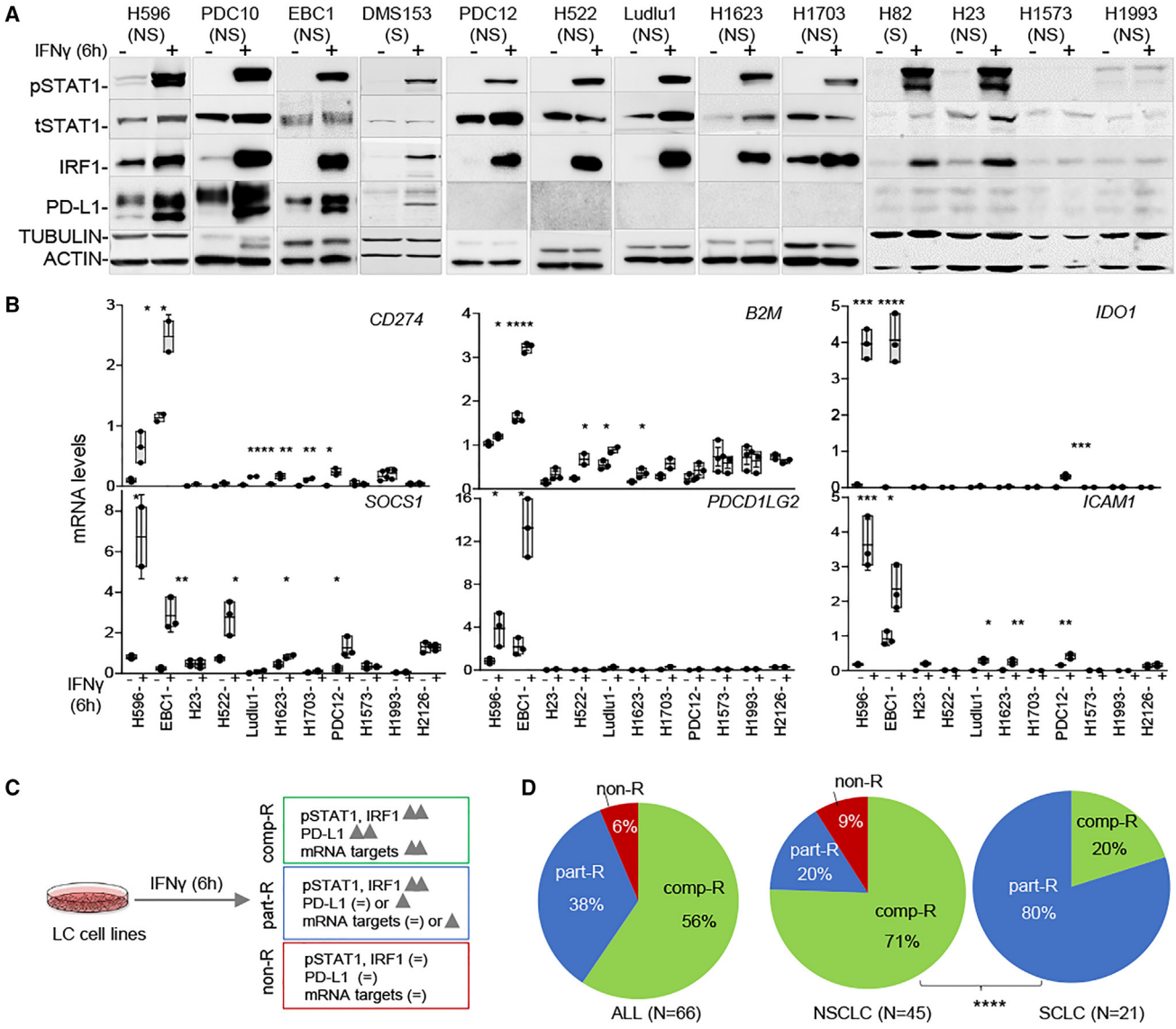

Figure 1. Abnormalities in the response to IFNγ in LC cells

(A) Western blot of the indicated proteins and cell lines, under basal conditions and after administering IFNγ (30 nM). The western blot of PD-L1 distinguishes two separate bands, the most abundant at 45 kDa and the other at 33 kDa. Both correspond to PD-L1, with the upper band being associated with an extensively N-glycosylated protein.[2,16] ACTIN and TUBULIN, protein-loading controls.

(B) mRNA levels assessed by real-time quantitative PCR of the indicated transcripts (relative to ACTIN) in the indicated NSCLC cells under basal conditions and after administering IFNγ. Results are presented as the median of independent biological triplicates. Asterisks denote statistical significance (*$p < 0.05$; **$p < 0.01$; ***$p < 0.005$; ****$p < 0.001$) from two-tailed Student's t tests. Data are presented as the mean ± SD.

(C) Scheme with the characteristics that define the three types of response to IFNγ in LC cells. Arrow, increase in levels; (=), no (or subtle) changes in levels.

(D) Distribution of each group in all LC cell lines (n = 55) and PDCs (n = 11) and among NSCLC and SCLC. Fisher's exact test (for comp-R and part-R groups). Asterisks denote statistical significance (****$p < 0.001$).

Comp-R, complete responders; non-R, non-responders; NS, NSCLC; part-R, partial responders; S, SCLC.

(Figure 2B), indicating that caution should be exercised when using high levels of PD-L1 as a marker for selecting patients for ICB-based treatments. We do not know whether the high levels of PD-L1 are due to the *IFNGR1* inactivation because the PDC11 cells have other genetic features, including a gene mutation in MAB21L2,[15] a member of the MAB21-like proteins that are related to the Stimulator of Interferon Genes (STING).[19]

We expressed *IFNGR1* wild type in the PDC11 cells, which restored the IFNγ signaling (Figures 2C and 2D). These results indicate that the genetic inactivation of *IFNGR1* abrogates the response to IFNγ, although it is infrequent in cancer, including LC.

Finally, we performed immunostaining to characterize the levels of IFNGR1 protein in a panel of 115 treatment-naive stage I–IIIA NSCLC primaries. About half of them showed little or no

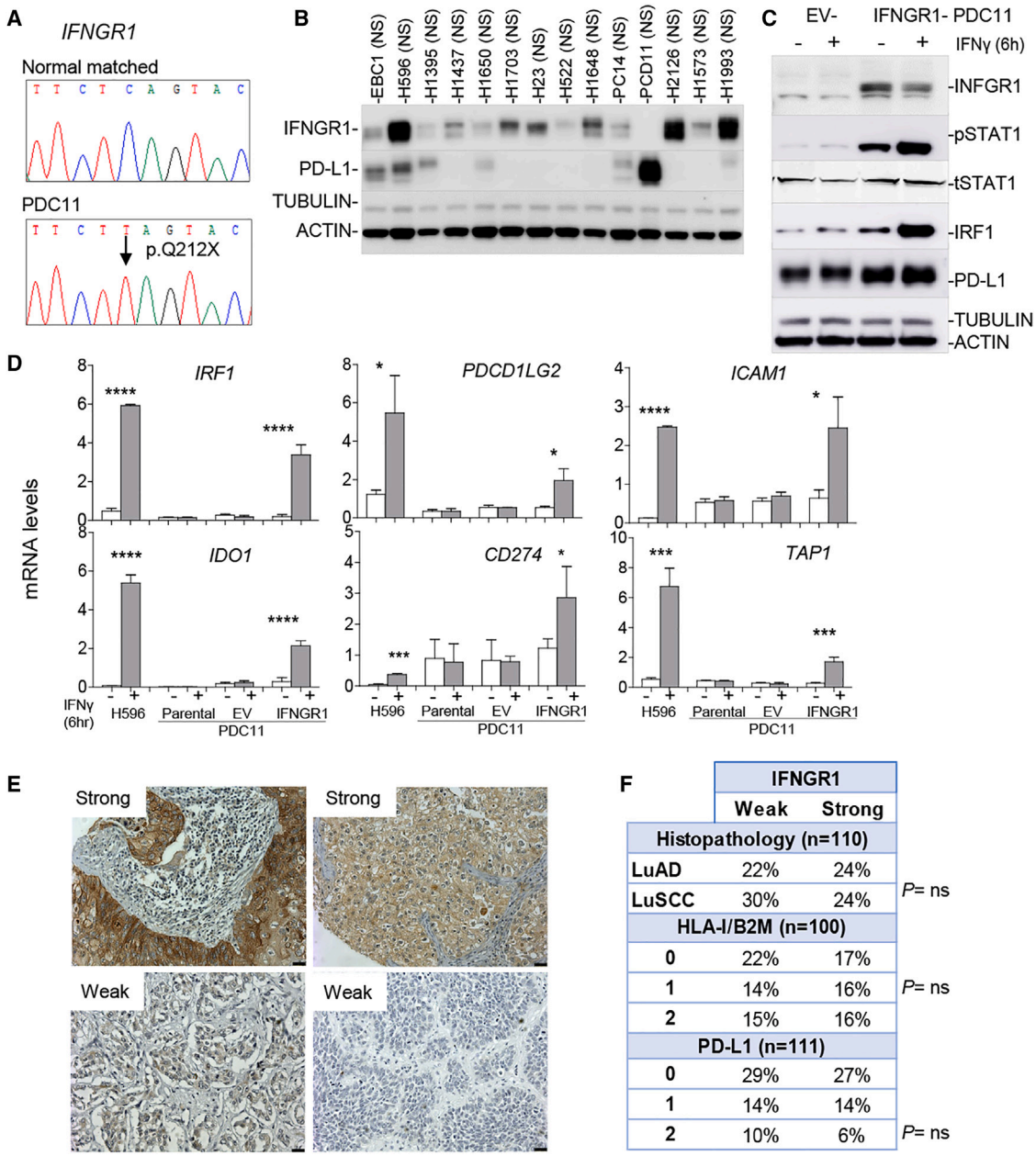

F

	IFNGR1	
	Weak	Strong
Histopathology (n=110)		
LuAD	22%	24%
LuSCC	30%	24%
		P= ns
HLA-I/B2M (n=100)		
0	22%	17%
1	14%	16%
2	15%	16%
		P= ns
PD-L1 (n=111)		
0	29%	27%
1	14%	14%
2	10%	6%
		P= ns

Figure 2. Genetic inactivation and expression of IFNγ receptor 1 (IFNGR1) in LC

(A) Chromatograms depicting, at the genomic level, the p.Q212X mutation at *IFNGR1* in PDC11 cells and the matched normal DNA. The nucleotide change is indicated by an arrow.

(B) Western blot of IFNGR1 and PD-L1 in the indicated LC cells. ACTIN and TUBULIN, protein-loading controls.

(C) Western blot showing changes in levels of the indicated proteins in the PCD11 cells expressing ectopic wild-type IFNGR1 (IFNGR1-PDC11) on treatment with IFNγ (30 nM), as compared with the empty vector (EV-PDC11) control. Experiments were independently repeated at least twice with similar results.

(D) mRNA levels assessed by real-time qPCR of the indicated transcripts (relative to *ACTIN*) under basal conditions and after administering IFNγ (30 nM), in H596 cells, in PCD11 parental cells (PDC11), in cells expressing ectopic wild-type IFNGR1 and in EV-PDC11 controls. Results are presented as the median of independent biological triplicates. Asterisks denote statistical significance (*p < 0.05; ***p < 0.005; ****p < 0.001) from two-tailed Student's t tests. Data are presented as the mean ± SD.

(E) Representative weak and strong immunostaining of IFNGR1 in lung primary tumors. Scale bars, 50 μm.

(F) Distribution of the immunostaining of IFNGR1 among lung tumors, by histopathology and levels of HLA-I/B2M and PD-L1. Fisher's exact test. ns, not significant,

LuAD, lung adenocarcinoma; LuSCC, lung squamous cell carcinoma; ns, not significant.

immunostaining of IFNGR1 (weak), whereas the other half showed a uniformly high level of staining (strong) (Figure 2E). No correlation was found between the levels of IFNGR1 and variables such as tumor histopathology or levels of HLA-I/B2M and PD-L1 proteins (Figure 2F), and there were no statistically significant differences in the overall survival of patients stratified by the tumor levels of IFNGR1 (Figure S2B). Likewise, the levels of IFNGR1 protein and its transcript were not associated with overall survival in cohorts of LC patients from public databases (Figure S2B).

Low basal levels of IγSGs occur in a subset of LC cells, associated in SCLCs with neuroendocrine characteristics

The aforementioned results indicate that the complete intrinsic abrogation of IFNγ signaling affects 5%–10% of the tumors, and that genetic inactivation of *JAK2* is the preferred mechanism. In contrast, about 38% of all LC cells, the part-R group (20% and 80% in NSCLC and SCLC, respectively), showed a transactivation-deficient stimulation by IFNγ (Figure 1D).

To understand the mechanisms that drive this deficiency, we interrogated an IFNγ signature (IFNγsign) from a previous study[2] in LC cells from the CCLE (n = 178). The analysis provided evidence of three main clusters (Figure 3A). Cluster I contained mostly SCLCs featuring neuroendocrine characteristics, i.e., high NEUROD1 and ASCL1 expressers, and the lowest levels of IFNγsign transcripts. Cluster II, composed mostly of comp-R and NSCLCs, showed the highest levels of genes from the IFNγsign. Finally, cluster III comprised a heterogeneous group of LC cells, including the non-R group, most of the non-neuroendocrine SCLCs (POU2F3 and YAP1 expressers), and most of the NSCLCs that are part-R. The latter cluster is characterized by intermediate expression of the IFNγsign transcripts. When a cohort of SCLC primaries[20] was interrogated for our IFNγsign, two groups were distinguished, the one with a higher level of expression being that containing most of the POU2F3-expressing tumors (Figure S3A). Together, these results highlight differences in the expression levels of IFNγsign transcripts between SCLCs, with those with neuroendocrine characteristics having a lower basal level of expression. Finally, we tested the IFNγsign in NSCLC primaries from the TCGA (n = 695), which discriminated two large clusters. The cluster with lower level of expression was highly enriched in lung squamous cell carcinomas (LuSCCs) ($p = 0.00001$) (Figure S3A).

Approximately half of the differentially expressed transcripts from the IFNγsign in the LC cells (CCLE), SCLC primary tumors,[20] and NSCLCs (TCGA) overlapped (Figure 3B). Most overlapping genes were well-established IγSGs, including many involved in immunorecognition, such as *B2M*, *HLAs*, *TAP1*, *TAP2*, and *TAPBP* (Tables S3–S5). Neuroendocrine SCLCs have intrinsically lower levels of immunoresponse-related proteins, including HLA-I.[8,26,27] Our observations support these previous results. Similarly, we found low levels of HLA-I/B2M proteins to be more common in LuSCCs.[8]

Together, the results reported above suggest that there is a subset of lung tumors that express low basal levels of genes from the IFNγsign. These include many SCLCs, especially the neuroendocrine type, and LuSCCs. The part-R cells also tend to feature low basal levels of these transcripts.

Histone 3 acetylation at lysine 27 (H3K27ac) in IγSG promoters is decreased among SCLCs with neuroendocrine characteristics

To delve deeper into the molecular basis of the low-level basal expression and of the sub-optimal global response to IFNγ in the part-R cells, we searched for changes in DNA methylation and histone modifications using genome-wide screening. Transcriptionally active chromatin domains are characterized by the absence of CpG methylation at the promoter regions and a distinct array of histone marks, e.g., H3K27ac, H3K4me1, and H3K4me3. Conversely, CpG promoter hypermethylation and H3K27me3 and H2AK119ub marks are often found at silent gene loci.[28] Here, we examined the DNA methylation database, available from the Sanger panel of cancer cell lines,[21] to search for aberrant hypermethylation at the IFNγsign genes in 177 LC cells, which could account for their lower basal expression. Aberrant hypermethylation at the promoters and 5′-end regulatory regions in association with a low level of expression was observed in eight genes ($R \leq -0.75$, $p < 0.05$) (Figures 3C and S3B). Hypermethylation at some of these promoters, e.g., *APOL1*, *CD74*, *TMEM106A*, and *TRIM38*, was more common in the part-R cells (Figure 3D). Thus, promoter hypermethylation at the 5′-end regulatory regions may underpin the lack of transcriptional activation on IFNγ treatment in a small subset of genes but is unlikely to explain the widespread sub-optimal transcriptional defects observed in the part-R cells.

Silencing basal HLA-I expression to restrict cytokine-induced upregulation has been shown in cancer cells mediated by the polycomb repressive complex 2 (PRC2).[29] Given this, we decided to test for possible differences in the accumulation of H3K27ac within the regulatory regions of the genes from the IFNγsign. We interrogated chromatin immunoprecipitation sequencing (ChIP-seq) datasets from six part-R (H23, H1048, H69, H446, DMS114, and H82) and two comp-R (A549 and H1299) LC cells, and one for which we do not have available information (H128). Among the SCLCs, there were two ASCL1 expressers (H128 and H69), two NEUROD1 expressers (H446 and H82), one YAP1 expresser (DMS114), and one POU2F3 expresser (H1048). As expected, there was a selectively high level of H3K27ac deposition at the promoters of each lineage transcription factor expressed in each cell line (Figure 3E). All NSCLC cells exhibited H3K27ac deposition at the YAP1 promoter. Compared with NSCLCs, SCLC cells, particularly the neuroendocrine (ASCL1 and NEUROD1 expresser), showed a lesser amount of H3K27ac in the promoters of the IFNγsign genes (Figure S4A). There were no apparent differences between the part-R and comp-R cells. An example of this is the promoters within the cluster containing four genes related to the response to IFNγ, i.e., *TAP1*, *TAP2*, *PSMB8*, and *PSMB9* (Figure 3F) and the *CD274* (Figure S4A). The lack of H3K27ac in the *TAP1/2-PSMB8/9* cluster in association with a low level of expression of the HLA-I complex has recently been reported in one SCLC cell, H69, which is an ASCL1 expresser that behaves like part-R in our screening.[30] We pre-treated some LC cells with SAHA, a histone deacetylase inhibitor, or with GSK126, an inhibitor of the H2K27 histone methyltransferase, EZH2, to determine whether a global increase in H3K27ac restores the response to IFNγ. The SAHA treatment increased

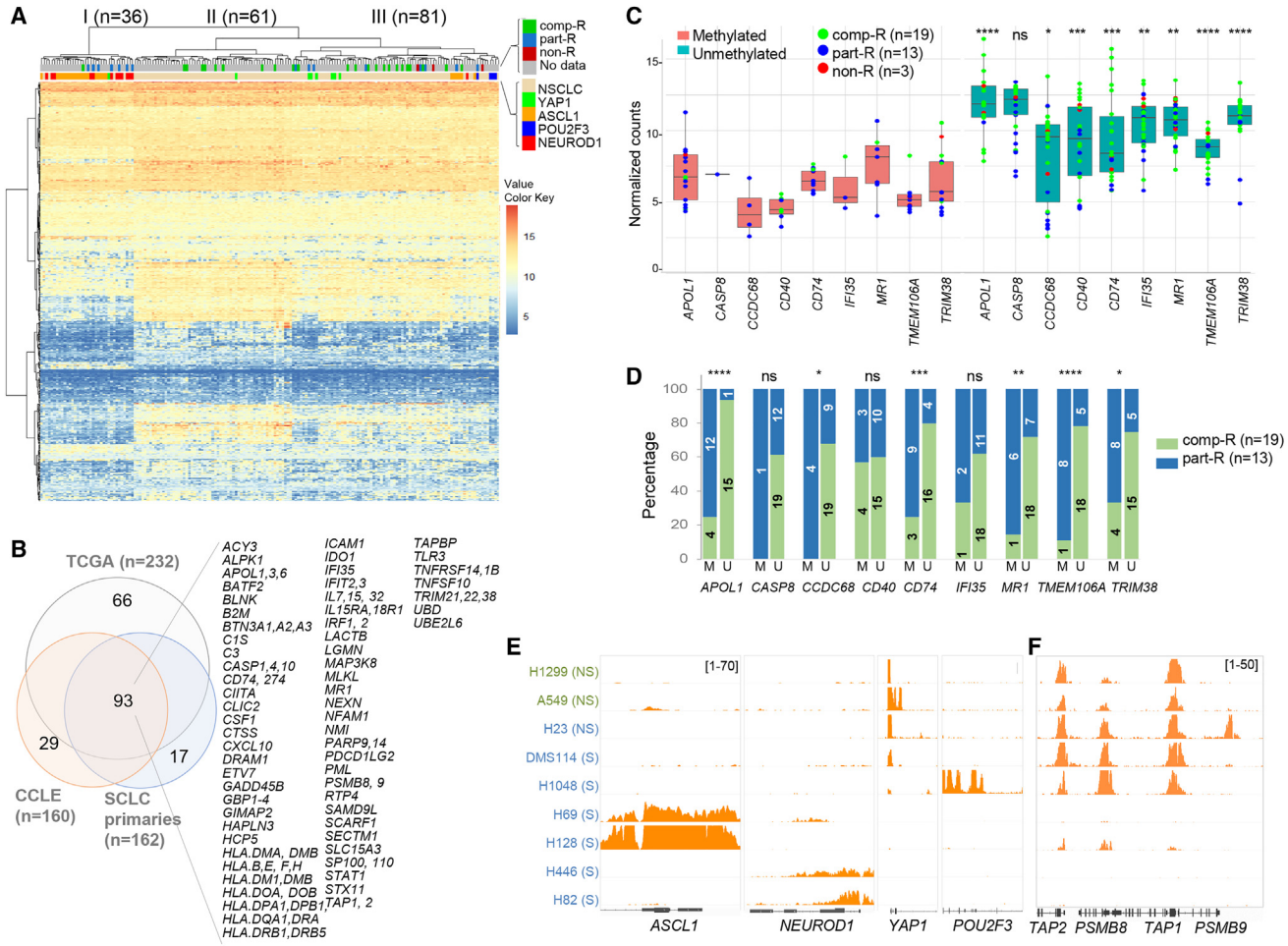

Figure 3. Reduced IFNγsign in part-R cells in the SCLC in association with neuroendocrine characteristics, with decreased H3K27ac and with promoter hypermethylation in a subset of genes

(A) Unsupervised hierarchical cluster and dendrograms, using the IFNγsign (from GEO: GSE109720), reflecting the gene expression profiles of the LC cell lines from the CCLE (https://sites.broadinstitute.org/ccle/). Heatmap for normalized counts. The type of response to IFNγ and LC are indicated.

(B) Venn diagrams showing overlap of the IFNγ sign transcripts, between those that are differentially expressed in clusters I and II of each indicated analysis. Depmap/CCLE database: https://depmap.org/portal/download/all/ (A; Table S3), SCLC primaries (Figure S3A; Table S4), and TCGA (lung primaries; Figure S3A; Table S5). All overlapping transcripts (n = 93) are listed.

(C) Boxplots depicting the expression levels of each indicated transcript in a set of LC cell lines from https://www.cbioportal.org/study/summary?id=ccle_broad_2019. Depmap/CCLE database: https://depmap.org/portal/download/all according to the methylated (mean $\beta \geq 0.66$) or unmethylated (mean $\beta < 0.66$) status of all the CpGs in the promoter regions (<2,000 bp away from a transcription start site [TSS]) from the Sanger panel of cancer cell lines (Table S1).[21] The type of response to IFNγ is also indicated. Two-tailed unpaired Student t tests compared the expression levels of each indicated transcript in the methylated versus unmethylated groups. In box-whisker plots, the horizontal band inside the box indicates the median, the bottom and top edges of the box indicate 25th–75th percentiles, and the whiskers indicate the minimum (min) to maximum (max). Asterisks denote statistical significance (*p < 0.05; **p < 0.01; ***p < 0.001; ****p < 0.0001). ns, not significant.

(D) Bar plot comparing the percentage of part-R or comp-R cells showing methylation (M) or unmethylation (U) at the promoter for each gene. The numbers inside the bars correspond to the number of LC cells in each group. Fisher's exact test. Asterisks denote statistical significance (*p < 0.05; **p < 0.01; ***p < 0.001; ****p < 0.0001). ns, not significant.

(E and F) Representative snapshots from the Integrative Genomics Viewer of ChIP-seq profiles of the H3K27ac at the indicated target loci and cancer cell lines (source GEO: GSE155129 for H1299;[22] GEO: GSE113715 for H23;[23] GEO: GSE175131 for A549[24] and GEO: GSE115124[25] for H1048, DMS114, H69, H82, H128, and H446). Names in green and blue refer to comp-R and part-R LC cells, respectively. NS, NSCLC; S, SCLC.

the levels of PD-L1 in the comp-R cells, but neither SAHA nor GSK126 completely reverted the deficient response to IFNγ in the part-R cells (Figure S4B). We also observed that SAHA was not capable of inducing H3K27ac in the H1299 cells.

Together, these findings indicate less extensive H3K27ac deposition in the promoter of genes from the IFNγsign in the SCLC cells of the neuroendocrine type (ASCL1- and NEUROD1-high expressers). This may be related to the low

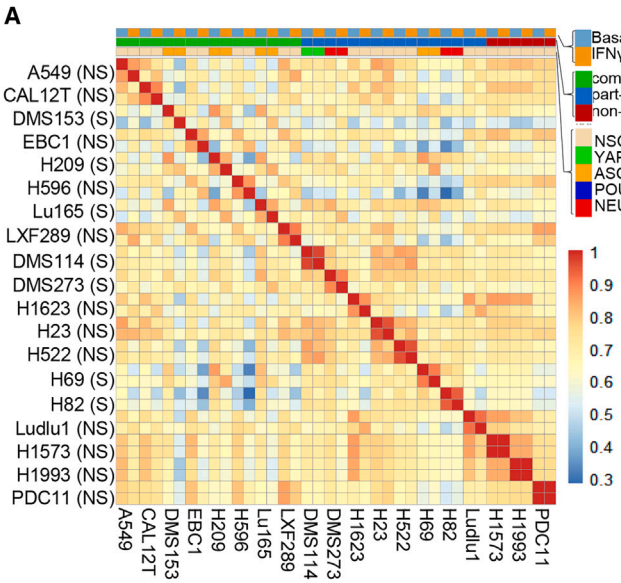

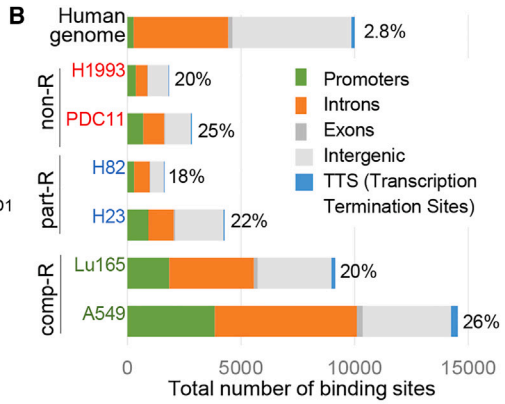

C

Cell line	Motif	Logo	E-Value	P-Value	Binding sites *	Back ground**
A549	AAAGTGA AASTR		5.4e-1870	2.0e-414	84.4%	4.4%
Lu165	GAAASTGA AAST		9.4e-2034	1.4e-239	85.1%	3.2%
H23	GAAAGTG AAAST		2.9e-1601	5.8e-083	62.7%	1.6%
H82	AAAGTGA AASTR		5.2e-1920	2.0e-026	82.3%	3.8%
H1993	AAAGTGA AASTR		1.3e-661	2.6e-009	32.1%	4.6%
PDC11	GAAAGTG AAAST		1.9e-1303	1.0e-018	75.9%	0.0%

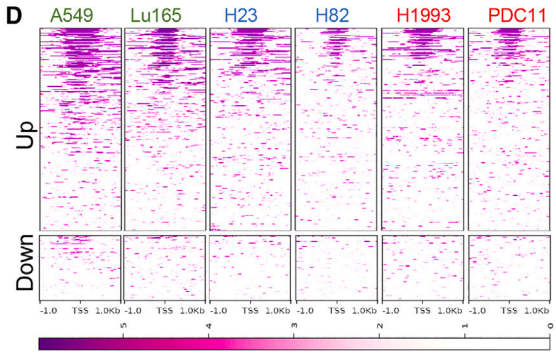

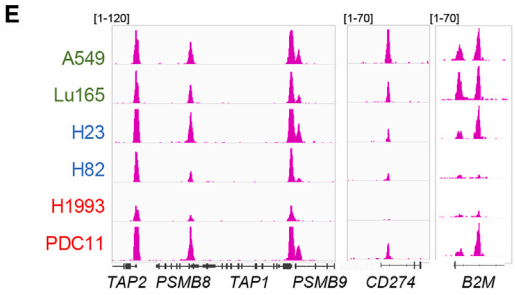

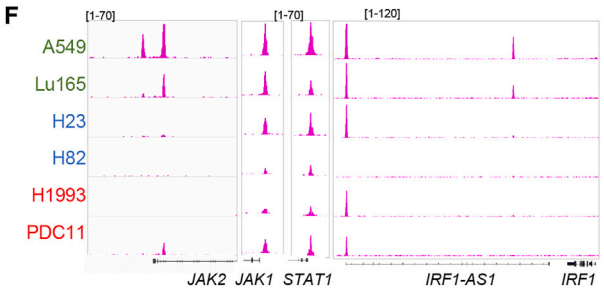

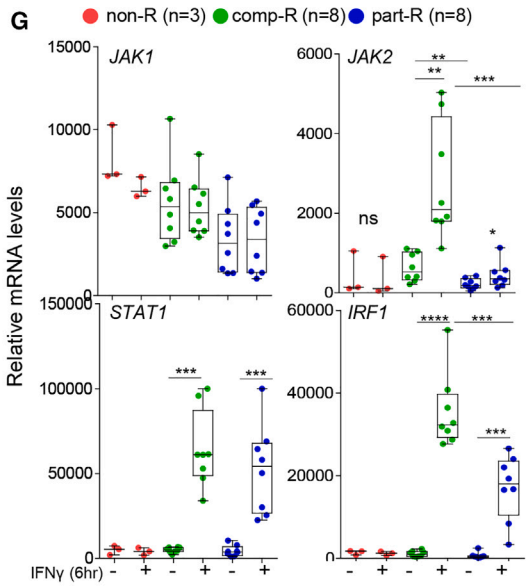

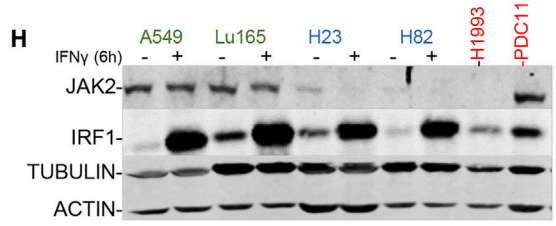

(legend on next page)

basal expression levels and sub-optimal IFNγ-mediated transactivation of these transcripts.

Cell-intrinsic transactivation and recruitment of IRF1 to the DNA by IFNγ is broadly deficient in part-R and non-R cells

To broadly assess the differential intrinsic response to IFNγ among LCs, we performed RNA-seq in a panel of comp-R, part-R, and non-R cells. In the non-Rs (*JAK2* and *IFNGR1* mutants), the administration of IFNγ did not upregulate the IγSGs, as expected. In the part-Rs, the transcriptional activation by IFNγ was sub-optimal, and the expression levels of IγSG transcripts barely changed (e.g., H82, H23, DMS114, H522, H69) (Figures 4A and S5A). Although the IFNγsign did not discriminate SCLCs from NSCLCs (Figure S5A), individual analysis of each cell line after IFNγ treatment revealed some differences in the upregulated IγSG transcripts between both histopathologies (Figure S5A). Further work will be required to validate this preliminary observation.

Downstream signaling by IFNγ involves phosphorylation of STAT1 and its translocation to the nucleus, to stimulate the expression of a set of genes, including transcription factor IRF1.[11,12] In contrast with the non-R cells, the part-R cells show activation of STAT1 and IRF1 following stimulation with IFNγ (Figure 1A). Given the low levels of H3K27ac deposition at IγSGs in some part-R cells (Figure S4A), we wondered whether the access of IRF1 to the DNA was limited. To establish the genome-wide binding profiles of IRF1, we performed ChIP-seq in a selected panel of LC cells (including two representatives each of the comp-R, part-R, and non-R cell types) after IFNγ stimulation. In all cells, around one-fifth of the regions that recruited IRF1 were within or near gene promoters, indicating that IRF1 was enriched in these regions (Figure 4B). There were fewer (half or less) IRF1-bound regions in the part-R (H23 and H82) and non-R (H1993 and PDC11) cells, compared with the comp-R cells (A549 and Lu165). A strong overlap between the promoter regions bound by IRF1 was observed in each of the cells (Figure S5B). *De novo* motif analysis showed the 5′-AAAGTGAAAST-3′ to be the core sequence that was strongly enriched in all the cells (Figures 4C and S5B). This is consistent with the IFN-stimulated response element (ISRE) 5'-GAAAnnGAAA-3', which is the consensus sequence for IRF1 and IRF2.[31]

The genes upregulated by IFNγ harbor IRF1 binding in their promoter regions, whereas downregulated genes do not show this association (Figure 4D). The results show that, despite a reduction in the overall number of peaks, IRF1 was bound to the same DNA regions in the non-R cells, probably contributing to the constitutive expression of the associated genes (Figures 4B and 4D). Consistent with that finding, the *IFNGR1*-deficient PDC11 cells, which express higher constitutive levels of PD-L1 and IγSGs transcripts than the *JAK2*-deficient H1993 (Figures 2B and S5A), also showed more IRF1-bound promoters (Figure 4B). This is also exemplified by the IRF1 targets, such as *TAP2*, *PSMB8*, *PSMB9*, *CD274*, and *B2M* (Figure 4E).

Inspection of specific regions of the genome showed that IRF1 is recruited to the promoters of genes involved in the IFNγ signal transduction pathway, such as *JAK1*, *JAK2*, and *STAT1* (Figure 4F). Although IRF1 was not bound to the *IRF1* promoter, a strong peak was evident upstream of an *IRF1-AS1* gene. The significance of this observation is unclear. The *JAK2*, *IRF1*, and *STAT1* transcripts became upregulated in the comp-R cells, and to a lesser extent in the part-R cells, on stimulation with IFNγ (Figure 4G). At the protein level, there were remarkably low levels of *JAK2* in the part-R cells compared with the comp-R cells (Figure 4H). This observation is consistent with a complete lack of recruitment of IRF1 to the promoter of *JAK2* in these cells (Figure 4F).

Collectively, these observations point to a similar reduction in the global DNA occupancy of IRF1 in the part-R cells as in the non-R cells. The lack of occupancy of IRF1 at the JAK2 promoter, coupled with the low level of constitutive expression of this protein in the part-R cells, may underlie the dysfunctional response to IFNγ in these cells.

Genetic activation of MYC represses the constitutive expression of JAK2 and impairs the response to IFNγ

SMARCA4, an ATPase of the SWI/SNF complex, is involved in the response to IFNγ. SMARCA4 is genetically inactivated in many LC cells,[32–34] including some of those in our study (Figure 5A; Table S1). We restituted the expression of SMARCA4 in part-R cells and found no changes in the response to IFNγ (Figure S6A). Further, at least two of the cells carrying genetic alterations at *JAK2* (non-R) also featured inactivation of

Figure 4. Deficient transactivation and recruitment of IRF1 to the DNA by IFNγ in part-R and non-R cells

(A) Heatmap of correlation matrix between the indicated LC cells, treated or untreated with IFNγ. The type of response to IFNγ and LC is indicated in the heatmap. The correlation coefficients are color-coded from deep red (1) to deep blue (0.3). NS, NSCLC; S, SCLC.

(B) Distribution of the IRF1 binding sites over genomic regions. Promoters are defined as the regions ±3 kb around the annotated TSSs. The percentage refers to the proportion of peaks at promoter regions.

(C) MEME *de novo* motif analysis in the IRF1 peaks for each indicated LC cell line revealed a highly significant abundance of the IRF1-associated motif (5'-GAAAnnGAAA-3'). Only the most significant motif of each cell line is shown. *Percentage of target sequences with motif of total targets. **Percentage of background sequences with motif of total background.

(D) Heatmaps representing the normalized ChIP-seq of IRF1 intensities plotted for the upregulated and downregulated genes of the IFNγsign. TSS, transcription start site.

(E and F) Representative snapshots from Integrative Genomics Viewer of ChIP-seq profiles of the IRF1 at the indicated target loci and cells.

(G) mRNA levels assessed by real-time quantitative PCR of the indicated transcripts (relative to *ACTIN*) in comp-R (green dots), part-R (blue dots), and non-R (red dots) cells under basal conditions (–) and on stimulation with IFNγ (30 nM) (+). Asterisks denote statistical significance (*$p < 0.05$; **$p < 0.01$; ***$p < 0.005$; ****$p < 0.001$) of two-tailed Student's t tests. Data are presented as the mean ± SD.

(H) Western blot of the indicated proteins and cancer cell lines, under basal conditions and after administering IFNγ. Experiments were independently repeated twice with similar results. ACTIN and TUBULIN, protein-loading controls. Names in green, blue, and red refer to comp-R, part-R, and non-R cells, respectively.

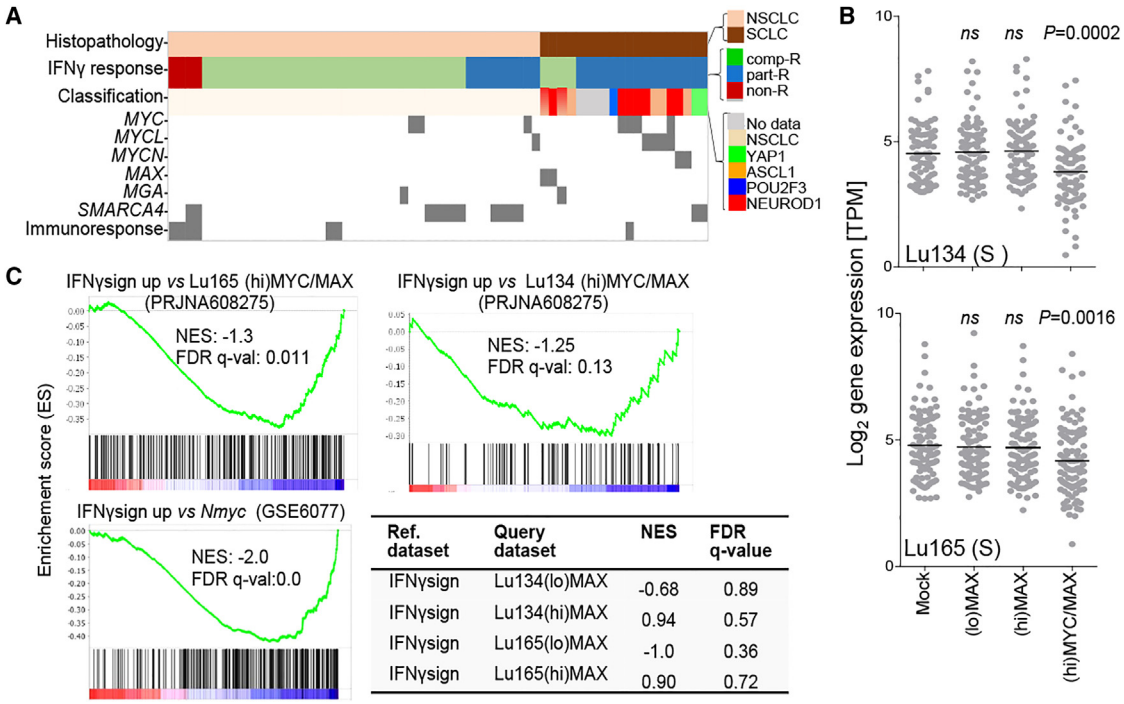

Ref. dataset	Query dataset	NES	FDR q-value
IFNγsign	Lu134(lo)MAX	-0.68	0.89
IFNγsign	Lu134(hi)MAX	0.94	0.57
IFNγsign	Lu165(lo)MAX	-1.0	0.36
IFNγsign	Lu165(hi)MAX	0.90	0.72

Figure 5. Oncogenic MYC and low level of constitutive expression of IFNγsign genes

(A) Oncoplot of the presence of alterations in the indicated genes. Immunoresponse indicates the presence of mutations of genes involved in immunorecognition (e.g., *B2M*, *TAP1/2*, *CALR*) or response to IFNγ (*JAK2* and *IFNGR1*)[2,8] and CCLE at cBioPortal.

(B) Graphs showing gene expression values in transcripts per million (TPMs) for the transcripts within the IFNγ signature from RNA-seq[2] and at GEO: GSE109720) in (lo)MAX-, (hi)MAX-, and (hi)MYC/MAX-expressing cells. Bars indicate means; differences assessed by two-sided Student's t test. ns, not significant; S, SCLC.

(C) Gene set enrichment analysis (GSEA) showing an inverse correlation in gene expression between the IFNγsign and datasets, including from lungs of mice overexpressing Nmyc (GEO: GSE6077).

FDR, false discovery rate; NES, normalized enrichment score.

SMARCA4. These results suggest the *SMARCA4* mutations do not play a major role in the attenuated response to IFNγ of the part-R cells.

We discovered that NEUROD1- and ASCL1-expressing SCLC cells, mostly part-R, have low basal expression levels of IFNγ sign genes (Figures 3A and S3A). These SCLC subtypes also commonly harbor amplification of the *MYC* family of genes.[35] Previously, we demonstrated that a subset of SCLC cells carries biallelic genetic inactivation of *MAX*, the obligate heterodimerization partner of the MYC proteins,[33] and more recently, we showed that the *MAX*-mutant cells are also classified among the ASCL1 or NEUROD1 subtypes.[36] It is striking that all nine SCLCs with activation of *MYC* were part-R, whereas those with genetic inactivation of *MAX* behaved like comp-R cells (Figure 5A). To explore whether MYC has a role in the low level of constitutive expression of IFNγsign genes and in the deficient response to IFNγ in the part-R cells, we used the isogenic cell models from *MAX*-deficient SCLC cells generated in our previous work.[36] These models consist of Lu134 or Lu165 cells that ectopically express, in a doxycycline-inducible manner, either only MAX at low [(lo)MAX] or high [(hi)MAX] levels, or both MYC and MAX simultaneously [(hi)MYC/MAX cells].[36] The latter express supra-physiological levels of MYC, with an MYC/MAX ratio very similar to that in *MYC*-amplified SCLC cells, thereby constituting a model of SCLC cells that have shifted from being MAX deficient to being MYC activated. We examined the RNA-seq data from these two isogenic models and observed a basal downregulation of transcripts from the IFNγsign in the SCLC cells carrying activation of MYC [(hi)MYC/MAX cells], but not in the mock, (lo)MAX, or (hi)MAX cells (Figures 5B and 5C). The IFNγsign was also downregulated in the lungs of mice carrying activated Nmyc (Figure 5C).

The oncogenic activation of MYC in SCLCs [(hi)MYC/MAX cells] led to a marked decrease in the basal levels of JAK2 and, to a lesser extent, of STAT1 and IRF1 (Figure 6A). It also prevented the upregulation of IγSGs when IFNγ was administered (Figure 6B). This did not happen in the (lo)MAX or (hi)MAX cells. Conversely, the depletion of MYC in three part-R, *MYC*-amplified LC cells (H2171, H446, and H460) increased the capability, in most of them, to upregulate the levels of JAK2 and various IγSGs, including *CD274*, on administration of IFNγ (Figure S6B). Altogether, these observations imply that MYC is involved in the intrinsic regulation of molecules that mediate the signaling through the IFNGR. Consistent with these observations, LC cells with amplified *MYC*, *MYCN*, or *MYCL1* showed significantly lower levels of *JAK2*, *STAT1*, and *IRF1* than their wild type counterparts (Figure 6C). We used the results of our previous ChIP sequencing of MYC and MAX in the different Lu134 and Lu165 cell models[36] and found some binding of MYC and MAX to the *JAK2* and *STAT1* promoters, although the intensity of the peaks was low compared with those of

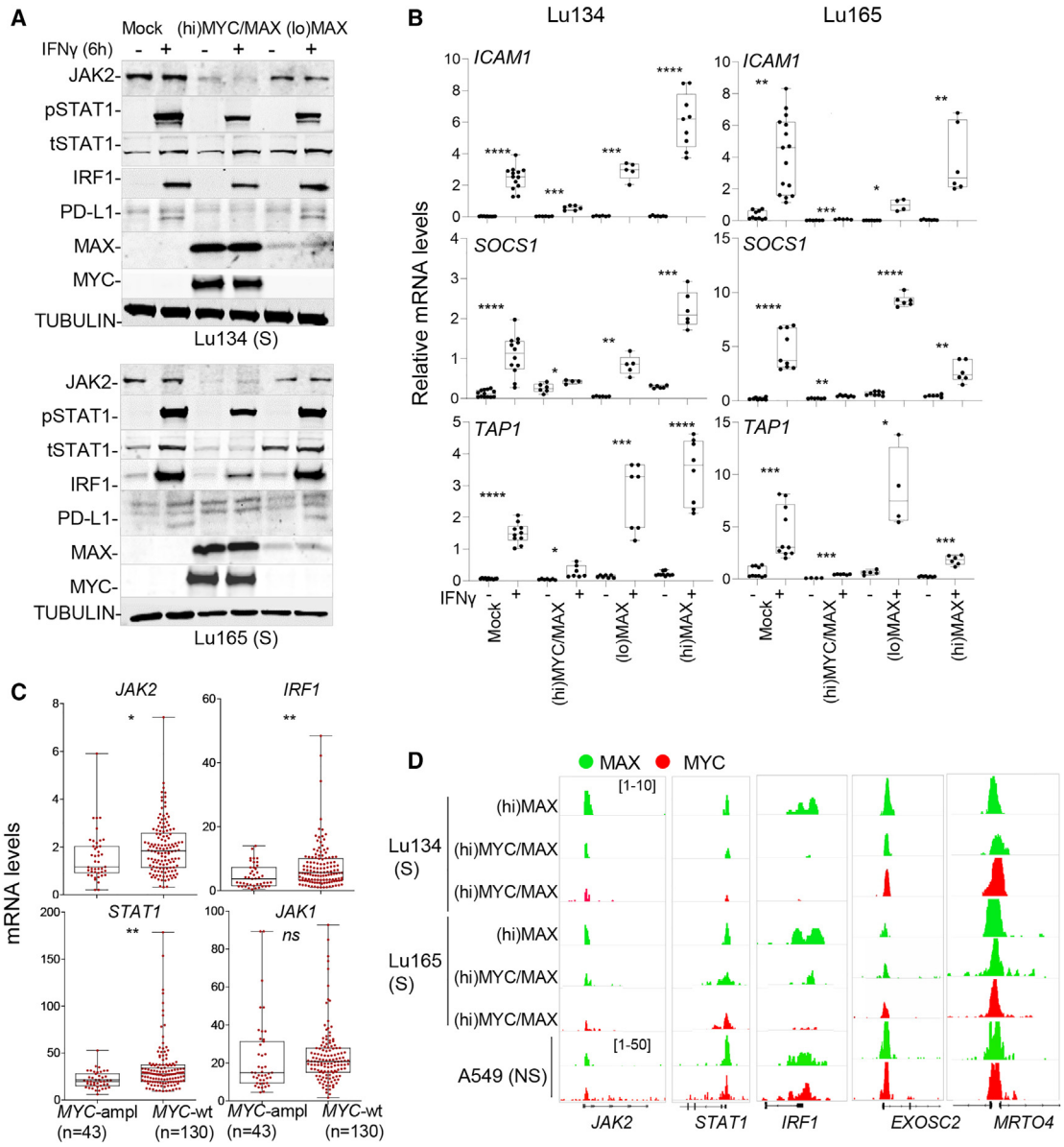

Figure 6. Oncogenic MYC impairs the response to IFNγ

(A) Western blot of the indicated proteins, LC cells, and genetic context [Mock, (hi)MYC/MAX, (lo)MAX] under basal conditions (−) and on treatment with IFNγ (30 nM) (+). Experiments were independently repeated twice with similar results. TUBULIN, protein-loading control. S, SCLC.

(B) mRNA levels assessed by real-time quantitative PCR of the indicated transcripts (relative to *IPO8*) in each SCLC cell line and genetic context: mock, (hi)MYC/MAX, (lo)MAX, and (hi)MAX, under basal conditions (−) and on treatment with IFNγ (30 nM) for 6 h (+). In box-whisker plots, the horizontal band inside the box indicates the median, the bottom and top edges of the box indicate 25th–75th percentiles, and the whiskers indicate the min to max. Asterisks denote statistical significance (*$p < 0.05$; **$p < 0.01$; ***$p < 0.005$; ****$p < 0.001$) from two-tailed Student's t tests. Data are presented as the mean ± SD.

(C) Plots comparing the mRNA levels of the indicated genes in LC cells (Depmap/CCLE database: https://depmap.org/portal/download/all) that have either *MYC*, *MYCL*, or *MYCN* amplification (*MYC*-ampl) or wild-type *MYC* (*MYC*-wt). Bars show the mean ± SD. Asterisks denote statistical significance (*$p < 0.05$; **$p < 0.01$; ns, not significant) from two-tailed Student's t tests.

(D) Representative snapshots from Integrative Genomics Viewer of ChIP-seq profiles of the MYC and MAX proteins at the indicated target locus and cells. *EXOSC2* and *MRTO4* are shown as positive controls for binding of MYC and MAX[36] (database: Sequence Read Archive, accession number BioProject: PRJNA608275).

the control regions for which MYC is a well-known transactivator (Figure 6D). We also gathered ChIP-seq information of MYC and MAX from the A549 cells, which are *MYC* wild type and comp-R, and found that MYC and MAX are bound to these promoters (Figure 6D). Finally, we observed that MYC was recruited to only about 15% of the promoters of genes that are upregulated by IFNγ and with low DNA-binding intensity (Figure S7), ruling out a global direct regulation of IγSGs by MYC.

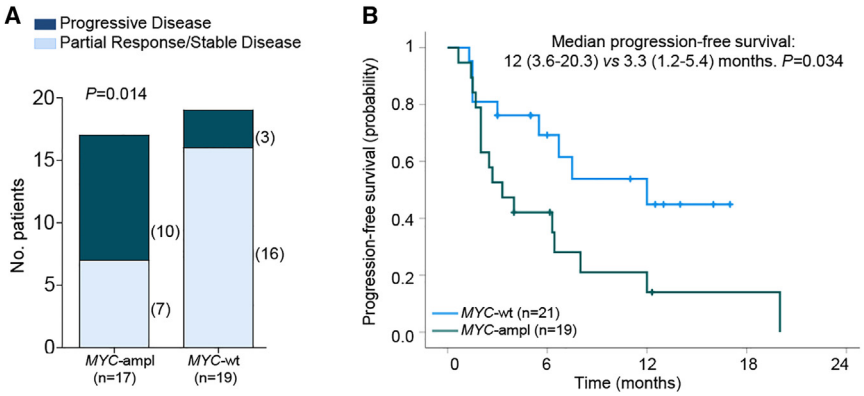

Figure 7. *MYC* amplification is associated with weaker response to ICB

(A) Bar plot showing the distribution of patients according to their response to the treatment in each of the *MYC*-ampl or *MYC*-wt groups. Fisher's exact test (comparing progressive disease vs. partial response/stable disease). Four patients were not evaluable for the overall rate of response (Table S6). (B) Kaplan-Meier curve showing progression-free survival after initiation of treatment with the immunotherapy according to the *MYC* copy number. Probabilities are those associated with the differences between the *MYC*-ampl and *MYC*-wt groups estimated by the log rank test.

Together, these findings attest to a role of oncogenic MYC in repressing IFNγ signaling, possibly by downregulating signal transduction molecules, particularly JAK2.

MYC amplification is associated with a worse response to ICB

We investigated whether the oncogenic activation of *MYC* in tumors from NSCLC patients can predict the therapeutic efficacy of ICBs. We included patients treated with anti-PD1 (pembrolizumab or nivolumab) in different combinations and with different lines of treatment (Table S6).

More than 120 NSCLC patients had been tested for tumor genome alterations using the Oncomine Comprehensive Assay Plus (OCA-Plus) or Oncomine Focus Assay (OFA) in the previous year in the Germans Trias i Pujol Hospital (Badalona, Spain). We also used an algorithm based on conumee to infer the *MYC*/*MYCN*/*MYCL1* copy number from DNA methylation arrays (http://bioconductor.org/packages/conumee/) in a previously profiled population of 89 NSCLC patients treated with ICBs.[37] A total of 19 NSCLC patients treated with ICBs and with *MYC*-amplified tumors were included in the study. As a control group, we considered consecutive patients treated with ICB with tumors negative for *MYC*-ampl (n = 21), selected from the genomic determination method OCA-plus (because the OFA approach does not determine the status of *MYCL1*) and with >50% tumor cell enrichment (Table S6).

First, we compared the response to ICBs of the two groups of LC patients according to the presence of either partial response (PR) or stable disease (SD), as measured by Response Evaluation Criteria In Solid Tumors (RECIST v.1.1 method). We found that patients harboring *MYC*-wt tumors showed a significantly greater clinical benefit to ICBs than did patients with *MYC*-ampl tumors (84% vs. 41% of PR/SD patients) (Figure 7A). Furthermore, patients whose tumors were categorized as *MYC*-wt had longer progression-free survival following immunotherapy than did those whose tumors were *MYC*-ampl (Figure 7B). Although they are preliminary, our results suggest that *MYC* status may serve as a biomarker to predict response to anti-PD (L)1 treatments.

DISCUSSION

Refractoriness to IFNγ has been demonstrated in some solid tumors, mainly melanoma, to be due to tumor-specific genetic alterations in molecules involved in the IFNγ signaling.[10,38] We previously showed inactivation at *JAK2* in a subset of LC cells[2] and now provide evidence of inactivation of *IFNGR1*, also associated with a lack of response to IFNγ, although this alteration was found to be rare. According to our current data from LC cells, tumor-specific genetic alterations that impair the host immune response, including the appropriate response to IFNγ and maturation of the HLA-I complex, affect about 15% of LCs. This frequency is likely to be underreported, given the difficulties in determining inactivation of the *HLA-I* genes arising from their highly polymorphic nature.[39] Hence it is appropriate to design clinical trials that set out to determine the role of these alterations in predicting the response to ICB.

Here, we also report that some LC cells, tentatively designated as part-R, have an intrinsic submaximal response to IFNγ defined as the markedly reduced transactivation of IγSGs. This deficiency was highly predominant in SCLCs, but not exclusive to them. Furthermore, and in agreement with previous reports,[40–42] we found low constitutive levels of IFNγsign genes, including B2M and HLAs, in a subset of LC cells and primary tumors, mainly in SCLCs with neuroendocrine characteristics.

Many SCLCs have long been known to have reduced levels of HLA-I complex,[26,27] and in a recent publication, Mahadevan et al.[30] reported low levels of HLA-I among neuroendocrine SCLCs in association with less durable benefits to the ICB. Here, we show that neuroendocrine SCLCs have less extensive accumulation of H3K27ac in the promoters from IFNγsign genes, which may explain their low level of constitutive expression. However, as has been shown,[30] the short-term administration of histone deacetylase inhibitors did not increase the levels of IFNγsign genes or the full response to IFNγ in the part-R cells.

When stimulated with IFNγ, the non-R and part-R cells show lower overall binding of IRF1 to the DNA compared with the comp-R. In the *JAK2* and *IFNGR1* mutant cells, IRF1 may contribute to the constitutive expression of its targets, presumably to the same extent as in IFNγ-untreated cells. Indeed, constitutive expression of IγSGs requires IRF1 binding.[43] It was interesting to observe that, in the comp-R cells, IRF1 occupied the promoter of *JAK2*. This did not happen in the part-R cells, which is consistent with the very low level of expression of JAK2 found in these cells. The low levels of JAK2 would prevent the full transactivation and global binding of IRF1 to the DNA

in the part-R cells, thereby reducing the transcriptional activation of IγSGs by IFNγ.

Although SMARCA4 and the SWI/SNF complex are known to mediate the response to IFNγ,[34] in our current work we did not find any direct involvement of SMARCA4 in the defects observed in the part-R cells. However, we did observe an association between the activation of the *MYC*-family of genes and a low level of constitutive expression of IγSGs and deficient stimulation by IFNγ. LCs with *MYC* amplification showed reduced levels of mediators of IFNγ signaling, whereas ectopic expression of oncogenic MYC in SCLC cells triggered the strong downregulation of JAK2 and of part-R features. All these observations are consistent with a role of oncogenic MYC in preventing stimulation by IFNγ. It has been known that IFNs inhibit cell growth involving c-myc repression,[44] whereas the ectopic expression of MYC overcomes IFNγ-mediated cell growth arrest,[45] indicating that MYC is involved in the inhibition of proliferation by IFNγ. The mechanisms underlying this function are not well known. In *Myc*-driven mouse models, the repressive MYC-MIZ1 complexes were found to transcriptionally repress the promoters of STAT1/2 in the type I IFN pathway.[46,47] Here, we found that ectopic oncogenic MYC is constitutively bound to the promoters of JAK2 and STAT1, although at a lower intensity, as compared with the control promoters. Thus, oncogenic MYC may repress various promoters associated with the response to IFNs (particularly that of JAK2) through the MYC-MIZ1 complexes. These complexes may prevent IRF1 from binding to these gene promoters. However, more work is needed to understand this phenomenon, because an indirect repression of JAK2 by MYC cannot be ruled out. Because MYC and MAX binding at these promoters was also observed in the comp-R and MYC wild-type A549 cells, the repressive action would occur only when MYC is genetically activated. Others have proposed a role for MYC in regulating the immune milieu. In preclinical studies, Myc promotes an immune-suppressive stroma that is obligatory for tumor progression,[48] and the inhibition of KRAS-G12C in LC upregulates IFN signaling via Myc inhibition.[49] Further, the depletion of MYC with epigenetic-based therapies increased IFN responsiveness and potentiated T cell attraction,[50] whereas MYC activation induced the secretion of immune-inhibitory cytokines.[51] These findings may be a consequence of the dysfunctional intrinsic regulation of the response to IFNs. It has been shown that MYC is sufficient to promote the conversion of classic SCLC to a variant morphology and to drive SCLC sequentially from an ASCL1 to a NEUROD1 to a non-neuroendocrine state.[52,53] It would be interesting to test whether these conversions are associated with changes in the response to IFNγ.

Finally, although our findings are preliminary, we suggest that the presence of *MYC* amplification in the tumor cells confers refractoriness to treatments with anti-PD1 and anti-PD-L1. In a previous study, activation of MYC, but not of MYCL or MYCN, was strongly associated with response to ICB,[41] and in triple-negative breast cancer patients receiving chemotherapy together with ICBs, a high MYC signature in the tumor tissues was associated with an increased probability of relapse or metastasis.[54] In this scenario, clinical trials are now required whose design enables them to determine the influence of these alterations, as well as that of genes involved in immunorecognition and the IFNγ pathway, as predictive markers in the response to ICB. It is likely that carrying out such trials will highlight the need to design appropriate genetic tests for patient selection in order to tailor their treatments using ICB strategies.

Limitations of the study

Although we report that oncogenic activation of the *MYC*-family of genes is involved in the observed disparity, on administration of IFNγ, between a proper signaling pathway activation and an impaired transcriptional response, the underlying mechanism is not fully elucidated. Although we propose that oncogenic MYC induces the repression of *JAK2*, it is still unclear whether this involves chromatin recruitment of MYC to the *JAK2* promoter. In addition, although the correlative studies point toward an involvement of all the different oncogenic MYC (MYC, MYCL, and MYCN) in this malfunction, the functional studies have been performed only with MYC. It will be important to reproduce these observations for oncogenic MYCL and MYCN. Finally, the number of *MYC*-amplified tumors from LC patients included in the study, to determine the association with a lack of response to treatment with ICB, is limited.

STAR★METHODS

Detailed methods are provided in the online version of this paper and include the following:

- KEY RESOURCES TABLE
- RESOURCE AVAILABILITY
  - Lead contact
  - Materials availability
  - Data availability
- EXPERIMENTAL MODEL AND SUBJECT DETAILS
  - Patients
- METHOD DETAILS
  - Antibodies, western blots and immunostainings
  - Construction of expression vectors and infections
  - Sanger sequencing of the *IFNGR1* gene
  - Quantitative real-time PCRs and RNA sequencing
  - Chromatin immunoprecipitation (ChIP)-sequencing of IRF1
  - Global methylation microarray analysis
- QUANTIFICATION AND STATISTICAL ANALYSIS
  - RNA sequencing data analysis
  - Chromatin immunoprecipitation (ChIP)-sequencing data analysis
  - Statistical analysis

SUPPLEMENTAL INFORMATION

Supplemental information can be found online at https://doi.org/10.1016/j.xcrm.2023.101006.

ACKNOWLEDGMENTS

The authors thank Isabel Bartolessis (Cancer Genetics Group) and Eva Mussolen (Cancer Epigenetics Group) at IJC for technical assistance. This work was

supported by Spanish grants from the MINECO (PID2020-114541RB-I00 to M.S.-C.) and from the Fundación Científica Asociación Española Contra el Cáncer (GCB14142170MONT to M.S.-C.). P.L. was supported by a fellowship from the Formación de Personal Investigador program (BES-2015-072204) and J.M.M. from the FI program AGAUR (2022 FI_B1 00085M). M.S. was supported by a Juan Rodes contract from the Instituto de Salud Carlos III (JR20/00015). O.A.R. was supported by an AECC contract (INVES19045ROME). We thank the CERCA Program/Generalitat de Catalunya for institutional support.

AUTHOR CONTRIBUTIONS

Conceptualization, M.S.-C.; methodology, J.J.A.-B., M.S., A.F.-A., J.M.M., A.V., O.A.R., E.P., and P.L.; formal analysis, P.N.-C., A.G., A.M.M.-M., P.B., M.T.-D., and A.E.-C.; investigation, J.J.A.-B., M.S., A.F.-A., J.M.M., A.V., O.A.R., E.P., and P.L.; resources, J.L.M., V.D., and M.E.; writing – original draft, M.S.-C.; writing – review & editing, M.S.-C., J.J.A.-B., M.S., E.P., and P.B.; visualization, J.J.A.-B., M.S., P.N.-C., and M.T.-D.; supervision, M.S.-C.; project administration, M.S.-C.; funding acquisition, M.S.-C.

DECLARATION OF INTERESTS

M.E. reports research grants from Ferrer International and Incyte and consulting fees from Quimatryx outside of the submitted work.

INCLUSION AND DIVERSITY

We support inclusive, diverse, and equitable conduct of research.

Received: June 1, 2022
Revised: July 29, 2022
Accepted: March 17, 2023
Published: April 11, 2023

REFERENCES

1. Chen, D.S., and Mellman, I. (2017). Elements of cancer immunity and the cancer–immune set point. Nature *541*, 321–330. https://doi.org/10.1038/nature21349.
2. Saigi, M., Alburquerque-Bejar, J.J., Mc Leer-Florin, A., Pereira, C., Pros, E., Romero, O.A., Baixeras, N., Esteve-Codina, A., Nadal, E., Brambilla, E., and Sanchez-Cespedes, M. (2018). *MET* -oncogenic and *JAK2* -inactivating alterations are independent factors that affect regulation of PD-L1 expression in lung cancer. Clin. Cancer Res. *24*, 4579–4587. https://doi.org/10.1158/1078-0432.CCR-18-0267.
3. Herbst, R.S., Morgensztern, D., and Boshoff, C. (2018). The biology and management of non-small cell lung cancer. Nature *553*, 446–454. https://doi.org/10.1038/nature25183.
4. Garassino, M.C., Gadgeel, S., Esteban, E., Felip, E., Speranza, G., Domine, M., Hochmair, M.J., Powell, S., Cheng, S.Y.-S., Bischoff, H.G., et al. (2020). Patient-reported outcomes following pembrolizumab or placebo plus pemetrexed and platinum in patients with previously untreated, metastatic, non-squamous non-small-cell lung cancer (KEYNOTE-189): a multicentre, double-blind, randomised, placebo-controlled, phase 3 trial. Lancet Oncol. *21*, 387–397. https://doi.org/10.1016/S1470-2045(19)30801-0.
5. Sugawara, S., Lee, J.-S., Kang, J.-H., Kim, H.R., Inui, N., Hida, T., Lee, K.H., Yoshida, T., Tanaka, H., Yang, C.-T., et al. (2021). Nivolumab with carboplatin, paclitaxel, and bevacizumab for first-line treatment of advanced nonsquamous non-small-cell lung cancer. Ann. Oncol. *32*, 1137–1147. https://doi.org/10.1016/j.annonc.2021.06.004.
6. Chan, T.A., Yarchoan, M., Jaffee, E., Swanton, C., Quezada, S.A., Stenzinger, A., and Peters, S. (2019). Development of tumor mutation burden as an immunotherapy biomarker: utility for the oncology clinic. Ann. Oncol. *30*, 44–56. https://doi.org/10.1093/annonc/mdy495.
7. Reck, M., Rodríguez-Abreu, D., Robinson, A.G., Hui, R., Csőszi, T., Fülöp, A., Gottfried, M., Peled, N., Tafreshi, A., Cuffe, S., et al. (2016). Pembrolizumab versus chemotherapy for PD-L1–positive non–small-cell lung cancer. N. Engl. J. Med. *375*, 1823–1833. https://doi.org/10.1056/NEJMoa1606774.
8. Pereira, C., Gimenez-Xavier, P., Pros, E., Pajares, M.J., Moro, M., Gomez, A., Navarro, A., Condom, E., Moran, S., Gomez-Lopez, G., et al. (2017). Genomic profiling of patient-derived xenografts for lung cancer identifies *B2M* inactivation impairing immunorecognition. Clin. Cancer Res. *23*, 3203–3213. https://doi.org/10.1158/1078-0432.CCR-16-1946.
9. Saigi, M., Alburquerque-Bejar, J.J., and Sanchez-Cespedes, M. (2019). Determinants of immunological evasion and immunocheckpoint inhibition response in non-small cell lung cancer: the genetic front. Oncogene *38*, 5921–5932. https://doi.org/10.1038/s41388-019-0855-x.
10. Gao, J., Shi, L.Z., Zhao, H., Chen, J., Xiong, L., He, Q., Chen, T., Roszik, J., Bernatchez, C., Woodman, S.E., et al. (2016). Loss of IFN-γ pathway genes in tumor cells as a mechanism of resistance to anti-CTLA-4 therapy. Cell *167*, 397–404.e9. https://doi.org/10.1016/j.cell.2016.08.069.
11. Schroder, K., Hertzog, P.J., Ravasi, T., and Hume, D.A. (2004). Interferon-gamma: an overview of signals, mechanisms and functions. J. Leukoc. Biol. *75*, 163–189. https://doi.org/10.1189/jlb.0603252.
12. Ivashkiv, L.B. (2018). IFNγ: signalling, epigenetics and roles in immunity, metabolism, disease and cancer immunotherapy. Nat. Rev. Immunol. *18*, 545–558. https://doi.org/10.1038/s41577-018-0029-z.
13. Ayers, M., Lunceford, J., Nebozhyn, M., Murphy, E., Loboda, A., Kaufman, D.R., Albright, A., Cheng, J.D., Kang, S.P., Shankaran, V., et al. (2017). IFN-γ–related mRNA profile predicts clinical response to PD-1 blockade. J. Clin. Invest. *127*, 2930–2940. https://doi.org/10.1172/JCI91190.
14. Binnewies, M., Roberts, E.W., Kersten, K., Chan, V., Fearon, D.F., Merad, M., Coussens, L.M., Gabrilovich, D.I., Ostrand-Rosenberg, S., Hedrick, C.C., et al. (2018). Understanding the tumor immune microenvironment (TIME) for effective therapy. Nat. Med. *24*, 541–550. https://doi.org/10.1038/s41591-018-0014-x.
15. Pros, E., Saigi, M., Alameda, D., Gomez-Mariano, G., Martinez-Delgado, B., Alburquerque-Bejar, J.J., Carretero, J., Tonda, R., Esteve-Codina, A., Catala, I., et al. (2020). Genome-wide profiling of non-smoking-related lung cancer cells reveals common RB1 rearrangements associated with histopathologic transformation in EGFR-mutant tumors. Ann. Oncol. *31*, 274–282. https://doi.org/10.1016/j.annonc.2019.09.001.
16. Li, C.-W., Lim, S.-O., Xia, W., Lee, H.-H., Chan, L.-C., Kuo, C.-W., Khoo, K.-H., Chang, S.-S., Cha, J.-H., Kim, T., et al. (2016). Glycosylation and stabilization of programmed death ligand-1 suppresses T-cell activity. Nat. Commun. *7*, 12632. https://doi.org/10.1038/ncomms12632.
17. Zitvogel, L., Galluzzi, L., Kepp, O., Smyth, M.J., and Kroemer, G. (2015). Type I interferons in anticancer immunity. Nat. Rev. Immunol. *15*, 405–414. https://doi.org/10.1038/nri3845.
18. van de Vosse, E., and van Dissel, J.T. (2017). IFN-γR1 defects: mutation update and description of the *IFNGR1* variation database: van de VOSSE and van DISSEL. Hum. Mutat. *38*, 1286–1296. https://doi.org/10.1002/humu.23302.
19. Ablasser, A., and Chen, Z.J. (2019). cGAS in action: expanding roles in immunity and inflammation. Science *363*, eaat8657. https://doi.org/10.1126/science.aat8657.
20. George, J., Lim, J.S., Jang, S.J., Cun, Y., Ozretić, L., Kong, G., Leenders, F., Lu, X., Fernández-Cuesta, L., Bosco, G., et al. (2015). Comprehensive genomic profiles of small cell lung cancer. Nature *524*, 47–53. https://doi.org/10.1038/nature14664.
21. Iorio, F., Knijnenburg, T.A., Vis, D.J., Bignell, G.R., Menden, M.P., Schubert, M., Aben, N., Gonçalves, E., Barthorpe, S., Lightfoot, H., et al. (2016). A landscape of pharmacogenomic interactions in cancer. Cell *166*, 740–754. https://doi.org/10.1016/j.cell.2016.06.017.
22. Romero, O.A., Vilarrubi, A., Alburquerque-Bejar, J.J., Gomez, A., Andrades, A., Trastulli, D., Pros, E., Setien, F., Verdura, S., Farré, L., et al.

(2021). SMARCA4 deficient tumours are vulnerable to KDM6A/UTX and KDM6B/JMJD3 blockade. Nat. Commun. *12*, 4319. https://doi.org/10.1038/s41467-021-24618-3.

23. Handoko, L., Kaczkowski, B., Hon, C.-C., Lizio, M., Wakamori, M., Matsuda, T., Ito, T., Jeyamohan, P., Sato, Y., Sakamoto, K., et al. (2018). JQ1 affects BRD2-dependent and independent transcription regulation without disrupting H4-hyperacetylated chromatin states. Epigenetics *13*, 410–431. https://doi.org/10.1080/15592294.2018.1469891.
24. ENCODE Project Consortium (2012). An integrated encyclopedia of DNA elements in the human genome. Nature *489*, 57–74. https://doi.org/10.1038/nature11247.
25. Huang, Y.-H., Klingbeil, O., He, X.-Y., Wu, X.S., Arun, G., Lu, B., Somerville, T.D.D., Milazzo, J.P., Wilkinson, J.E., Demerdash, O.E., et al. (2018). POU2F3 is a master regulator of a tuft cell-like variant of small cell lung cancer. Genes Dev. *32*, 915–928. https://doi.org/10.1101/gad.314815.118.
26. Doyle, A., Martin, W.J., Funa, K., Gazdar, A., Carney, D., Martin, S.E., Linnoila, I., Cuttitta, F., Mulshine, J., and Bunn, P. (1985). Markedly decreased expression of class I histocompatibility antigens, protein, and mRNA in human small-cell lung cancer. J. Exp. Med. *161*, 1135–1151. https://doi.org/10.1084/jem.161.5.1135.
27. Funa, K., Gazdar, A.F., Minna, J.D., and Linnoila, R.I. (1986). Paucity of beta 2-microglobulin expression on small cell lung cancer, bronchial carcinoids and certain other neuroendocrine tumors. Lab. Invest. *55*, 186–193.
28. Tessarz, P., and Kouzarides, T. (2014). Histone core modifications regulating nucleosome structure and dynamics. Nat. Rev. Mol. Cell Biol. *15*, 703–708. https://doi.org/10.1038/nrm3890.
29. Burr, M.L., Sparbier, C.E., Chan, K.L., Chan, Y.-C., Kersbergen, A., Lam, E.Y.N., Azidis-Yates, E., Vassiliadis, D., Bell, C.C., Gilan, O., et al. (2019). An evolutionarily conserved function of polycomb silences the MHC class I antigen presentation pathway and enables immune evasion in cancer. Cancer Cell *36*, 385–401.e8. https://doi.org/10.1016/j.ccell.2019.08.008.
30. Mahadevan, N.R., Knelson, E.H., Wolff, J.O., Vajdi, A., Saigí, M., Campisi, M., Hong, D., Thai, T.C., Piel, B., Han, S., et al. (2021). Intrinsic immunogenicity of small cell lung carcinoma revealed by its cellular plasticity. Cancer Discov. *11*, 1952–1969. https://doi.org/10.1158/2159-8290.CD-20-0913.
31. Harada, H., Fujita, T., Miyamoto, M., Kimura, Y., Maruyama, M., Furia, A., Miyata, T., and Taniguchi, T. (1989). Structurally similar but functionally distinct factors, IRF-1 and IRF-2, bind to the same regulatory elements of IFN and IFN-inducible genes. Cell *58*, 729–739. https://doi.org/10.1016/0092-8674(89)90107-4.
32. Medina, P.P., Romero, O.A., Kohno, T., Montuenga, L.M., Pio, R., Yokota, J., and Sanchez-Cespedes, M. (2008). Frequent BRG1/SMARCA4-inactivating mutations in human lung cancer cell lines. Hum. Mutat. *29*, 617–622. https://doi.org/10.1002/humu.20730.
33. Romero, O.A., Torres-Diz, M., Pros, E., Savola, S., Gomez, A., Moran, S., Saez, C., Iwakawa, R., Villanueva, A., Montuenga, L.M., et al. (2014). *MAX* inactivation in small cell lung cancer disrupts MYC–SWI/SNF programs and is synthetic lethal with BRG1. Cancer Discov. *4*, 292–303. https://doi.org/10.1158/2159-8290.CD-13-0799.
34. Liu, H., Kang, H., Liu, R., Chen, X., and Zhao, K. (2002). Maximal induction of a subset of interferon target genes requires the chromatin-remodeling activity of the BAF complex. Mol. Cell Biol. *22*, 6471–6479. https://doi.org/10.1128/MCB.22.18.6471-6479.2002.
35. Rudin, C.M., Poirier, J.T., Byers, L.A., Dive, C., Dowlati, A., George, J., Heymach, J.V., Johnson, J.E., Lehman, J.M., MacPherson, D., et al. (2019). Molecular subtypes of small cell lung cancer: a synthesis of human and mouse model data. Nat. Rev. Cancer *19*, 289–297. https://doi.org/10.1038/s41568-019-0133-9.
36. Llabata, P., Torres-Diz, M., Gomez, A., Tomas-Daza, L., Romero, O.A., Grego-Bessa, J., Llinas-Arias, P., Valencia, A., Esteller, M., Javierre, B.M., et al. (2021). MAX mutant small-cell lung cancers exhibit impaired activities of MGA-dependent noncanonical polycomb repressive complex. Proc. Natl. Acad. Sci. USA *118*, e2024824118. https://doi.org/10.1073/pnas.2024824118.
37. Duruisseaux, M., Martínez-Cardús, A., Calleja-Cervantes, M.E., Moran, S., Castro de Moura, M., Davalos, V., Piñeyro, D., Sanchez-Cespedes, M., Girard, N., Brevet, M., et al. (2018). Epigenetic prediction of response to anti-PD-1 treatment in non-small-cell lung cancer: a multicentre, retrospective analysis. Lancet Respir. Med. *6*, 771–781. https://doi.org/10.1016/S2213-2600(18)30284-4.
38. Shin, D.S., Zaretsky, J.M., Escuin-Ordinas, H., Garcia-Diaz, A., Hu-Lieskovan, S., Kalbasi, A., Grasso, C.S., Hugo, W., Sandoval, S., Torrejon, D.Y., et al. (2017). Primary resistance to PD-1 blockade mediated by *JAK1/2* mutations. Cancer Discov. *7*, 188–201. https://doi.org/10.1158/2159-8290.CD-16-1223.
39. Shukla, S.A., Rooney, M.S., Rajasagi, M., Tiao, G., Dixon, P.M., Lawrence, M.S., Stevens, J., Lane, W.J., Dellagatta, J.L., Steelman, S., et al. (2015). Comprehensive analysis of cancer-associated somatic mutations in class I HLA genes. Nat. Biotechnol. *33*, 1152–1158. https://doi.org/10.1038/nbt.3344.
40. Gay, C.M., Stewart, C.A., Park, E.M., Diao, L., Groves, S.M., Heeke, S., Nabet, B.Y., Fujimoto, J., Solis, L.M., Lu, W., et al. (2021). Patterns of transcription factor programs and immune pathway activation define four major subtypes of SCLC with distinct therapeutic vulnerabilities. Cancer Cell *39*, 346–360.e7. https://doi.org/10.1016/j.ccell.2020.12.014.
41. Roper, N., Velez, M.J., Chiappori, A., Kim, Y.S., Wei, J.S., Sindiri, S., Takahashi, N., Mulford, D., Kumar, S., Ylaya, K., et al. (2021). Notch signaling and efficacy of PD-1/PD-L1 blockade in relapsed small cell lung cancer. Nat. Commun. *12*, 3880. https://doi.org/10.1038/s41467-021-24164-y.
42. Owonikoko, T.K., Dwivedi, B., Chen, Z., Zhang, C., Barwick, B., Ernani, V., Zhang, G., Gilbert-Ross, M., Carlisle, J., Khuri, F.R., et al. (2021). YAP1 expression in SCLC defines a distinct subtype with T-cell–inflamed phenotype. J. Thorac. Oncol. *16*, 464–476. https://doi.org/10.1016/j.jtho.2020.11.006.
43. Langlais, D., Barreiro, L.B., and Gros, P. (2016). The macrophage IRF8/IRF1 regulome is required for protection against infections and is associated with chronic inflammation. J. Exp. Med. *213*, 585–603. https://doi.org/10.1084/jem.20151764.
44. Stark, G.R., Kerr, I.M., Williams, B.R., Silverman, R.H., and Schreiber, R.D. (1998). HOW cells respond to interferons. Annu. Rev. Biochem. *67*, 227–264. https://doi.org/10.1146/annurev.biochem.67.1.227.
45. Vairo, G., Vadiveloo, P.K., Royston, A.K., Rockman, S.P., Rock, C.O., Jackowski, S., and Hamilton, J.A. (1995). Deregulated c-myc expression overrides IFN gamma-induced macrophage growth arrest. Oncogene *10*, 1969–1976.
46. Muthalagu, N., Monteverde, T., Raffo-Iraolagoitia, X., Wiesheu, R., Whyte, D., Hedley, A., Laing, S., Kruspig, B., Upstill-Goddard, R., Shaw, R., et al. (2020). Repression of the type I interferon pathway underlies MYC- and KRAS-dependent evasion of NK and B cells in pancreatic ductal adenocarcinoma. Cancer Discov. *10*, 872–887. https://doi.org/10.1158/2159-8290.CD-19-0620.
47. Swaminathan, S., Hansen, A.S., Heftdal, L.D., Dhanasekaran, R., Deutzmann, A., Fernandez, W.D.M., Liefwalker, D.F., Horton, C., Mosley, A., Liebersbach, M., et al. (2020). MYC functions as a switch for natural killer cell-mediated immune surveillance of lymphoid malignancies. Nat. Commun. *11*, 2860. https://doi.org/10.1038/s41467-020-16447-7.
48. Kortlever, R.M., Sodir, N.M., Wilson, C.H., Burkhart, D.L., Pellegrinet, L., Brown Swigart, L., Littlewood, T.D., and Evan, G.I. (2017). Myc cooperates with ras by programming inflammation and immune suppression. Cell *171*, 1301–1315.e14. https://doi.org/10.1016/j.cell.2017.11.013.
49. Mugarza, E., van Maldegem, F., Boumelha, J., Moore, C., Rana, S., Llorian Sopena, M., East, P., Ambler, R., Anastasiou, P., Romero-Clavijo, P., et al. (2022). Therapeutic KRAS ^{G12C} inhibition drives effective interferon-mediated antitumor immunity in immunogenic lung cancers. Sci. Adv. *8*, eabm8780. https://doi.org/10.1126/sciadv.abm8780.

50. Topper, M.J., Vaz, M., Chiappinelli, K.B., DeStefano Shields, C.E., Niknafs, N., Yen, R.-W.C., Wenzel, A., Hicks, J., Ballew, M., Stone, M., et al. (2017). Epigenetic therapy ties MYC depletion to reversing immune evasion and treating lung cancer. Cell *171*, 1284–1300.e21. https://doi.org/10.1016/j.cell.2017.10.022.

51. Reimann, M., Lee, S., Loddenkemper, C., Dörr, J.R., Tabor, V., Aichele, P., Stein, H., Dörken, B., Jenuwein, T., and Schmitt, C.A. (2010). Tumor stroma-derived TGF-β limits myc-driven lymphomagenesis via suv39h1-dependent senescence. Cancer Cell *17*, 262–272. https://doi.org/10.1016/j.ccr.2009.12.043.

52. Mollaoglu, G., Jones, A., Wait, S.J., Mukhopadhyay, A., Jeong, S., Arya, R., Camolotto, S.A., Mosbruger, T.L., Stubben, C.J., Conley, C.J., et al. (2018). The lineage-defining transcription factors SOX2 and NKX2-1 determine lung cancer cell fate and shape the tumor immune microenvironment. Immunity *49*, 764–779.e9. https://doi.org/10.1016/j.immuni.2018.09.020.

53. Ireland, A.S., Micinski, A.M., Kastner, D.W., Guo, B., Wait, S.J., Spainhower, K.B., Conley, C.C., Chen, O.S., Guthrie, M.R., Soltero, D., et al. (2020). MYC drives temporal evolution of small cell lung cancer subtypes by reprogramming neuroendocrine fate. Cancer Cell *38*, 60–78.e12. https://doi.org/10.1016/j.ccell.2020.05.001.

54. Lee, J.V., Housley, F., Yau, C., Nakagawa, R., Winkler, J., Anttila, J.M., Munne, P.M., Savelius, M., Houlahan, K.E., Van de Mark, D., et al. (2022). Combinatorial immunotherapies overcome MYC-driven immune evasion in triple negative breast cancer. Nat. Commun. *13*, 3671. https://doi.org/10.1038/s41467-022-31238-y.

55. Subramanian, A., Tamayo, P., Mootha, V.K., Mukherjee, S., Ebert, B.L., Gillette, M.A., Paulovich, A., Pomeroy, S.L., Golub, T.R., Lander, E.S., and Mesirov, J.P. (2005). Gene set enrichment analysis: a knowledge-based approach for interpreting genome-wide expression profiles. Proc. Natl. Acad. Sci. USA *102*, 15545–15550. https://doi.org/10.1073/pnas.0506580102.

56. Dobin, A., Davis, C.A., Schlesinger, F., Drenkow, J., Zaleski, C., Jha, S., Batut, P., Chaisson, M., and Gingeras, T.R. (2013). STAR: ultrafast universal RNA-seq aligner. Bioinformatics *29*, 15–21. https://doi.org/10.1093/bioinformatics/bts635.

57. Li, B., and Dewey, C.N. (2011). RSEM: accurate transcript quantification from RNA-Seq data with or without a reference genome. BMC Bioinf. *12*, 323. https://doi.org/10.1186/1471-2105-12-323.

58. Law, C.W., Chen, Y., Shi, W., and Smyth, G.K. (2014). voom: precision weights unlock linear model analysis tools for RNA-seq read counts. Genome Biol. *15*, R29. https://doi.org/10.1186/gb-2014-15-2-r29.

59. Raudvere, U., Kolberg, L., Kuzmin, I., Arak, T., Adler, P., Peterson, H., and Vilo, J. (2019). g:Profiler: a web server for functional enrichment analysis and conversions of gene lists (2019 update). Nucleic Acids Res. *47*, W191–W198. https://doi.org/10.1093/nar/gkz369.

60. Love, M.I., Huber, W., and Anders, S. (2014). Moderated estimation of fold change and dispersion for RNA-seq data with DESeq2. Genome Biol. *15*, 550. https://doi.org/10.1186/s13059-014-0550-8.

61. Andrews, S. (2010). FastQC: A Quality Control Tool for High Throughput Sequence Data. http://www.bioinformatics.babraham.ac.uk/projects/fastqc.

62. Jiang, H., Lei, R., Ding, S.-W., and Zhu, S. (2014). Skewer: a fast and accurate adapter trimmer for next-generation sequencing paired-end reads. BMC Bioinf. *15*, 182. https://doi.org/10.1186/1471-2105-15-182.

63. Langmead, B., and Salzberg, S.L. (2012). Fast gapped-read alignment with Bowtie 2. Nat. Methods *9*, 357–359. https://doi.org/10.1038/nmeth.1923.

64. Zhang, Y., Liu, T., Meyer, C.A., Eeckhoute, J., Johnson, D.S., Bernstein, B.E., Nusbaum, C., Myers, R.M., Brown, M., Li, W., and Liu, X.S. (2008). Model-based analysis of ChIP-seq (MACS). Genome Biol. *9*, R137. https://doi.org/10.1186/gb-2008-9-9-r137.

65. Heinz, S., Benner, C., Spann, N., Bertolino, E., Lin, Y.C., Laslo, P., Cheng, J.X., Murre, C., Singh, H., and Glass, C.K. (2010). Simple combinations of lineage-determining transcription factors prime cis-regulatory elements required for macrophage and B cell identities. Mol. Cell *38*, 576–589. https://doi.org/10.1016/j.molcel.2010.05.004.

66. Ramírez, F., Ryan, D.P., Grüning, B., Bhardwaj, V., Kilpert, F., Richter, A.S., Heyne, S., Dündar, F., and Manke, T. (2016). deepTools2: a next generation web server for deep-sequencing data analysis. Nucleic Acids Res. *44*, W160–W165. https://doi.org/10.1093/nar/gkw257.

67. Machanick, P., and Bailey, T.L. (2011). MEME-ChIP: motif analysis of large DNA datasets. Bioinformatics *27*, 1696–1697. https://doi.org/10.1093/bioinformatics/btr189.

68. Pérez-Salvia, M., Simó-Riudalbas, L., Llinàs-Arias, P., Roa, L., Setien, F., Soler, M., de Moura, M.C., Bradner, J.E., Gonzalez-Suarez, E., Moutinho, C., and Esteller, M. (2017). Bromodomain inhibition shows antitumoral activity in mice and human luminal breast cancer. Oncotarget *8*, 51621–51629. https://doi.org/10.18632/oncotarget.18255.

STAR★METHODS

KEY RESOURCES TABLE

REAGENT or RESOURCE	SOURCE	IDENTIFIER
Antibodies		
pSTAT1	Cell Signaling	Cat# 9167; RRID:AB_561284
STAT1	Cell Signaling	Cat# 9175; RRID:AB_2197984
IRF1	Cell Signaling	Cat# 8478; RRID:AB_10949108
PD-L1	Cell Signaling	Cat# 13684; RRID:AB_2687655
IFNgR1	Proteintech	Cat# 10808-1-AP; RRID:AB_2121604
IFNgR1	Abcam	Cat# ab154400; RRID: NA
ACTIN	Sigma-Aldrich	Cat# A1978; RRID:AB_476692
TUBULIN	ROCKLAND	Cat# (17H11.F10) - 200-301-880; RRID:AB_10705001
H3K27me3	Sigma-Aldrich	Cat# 07–449; RRID:AB_310624
H3K27ac	Cell Signaling	Cat# 8173 (D5E4); RRID:AB_10949503
Histone 3	Cell Signaling	Cat# 9715; RRID:AB_331563
SMARCA4	Cell Signaling	Cat# 49360; RRID:AB_2728743
JAK2	Cell Signaling	Cat# 3230; RRID:AB_2128522
MYC	Cell Signaling	Cat# 13987; RRID:AB_2631168
MAX	Santa Cruz	Cat# sc-197 (C-17); RRID:AB_2281783
IRDye 680LT Donkey anti-Mouse IgG Secondary Antibody	LI-COR	Cat# 925–68022; RRID:AB_2814906
IRDye 800CW Donkey anti-Rabbit IgG Secondary Antibody	LI-COR	Cat# 925–32213; RRID:AB_2715510
Bacterial and virus strains		
Escherichia coli (E. coli) strain DH5α	Internal stock	N/A
Chemicals, peptides, and recombinant proteins		
RPMI 1640 Medium	Gibco	Cat# 61870044
DMEM Medium	Gibco	Cat# 61965059
Waymouth's Medium	Gibco	Cat# 31220023
McCoy's 5A (Modified) Medium	Gibco	Cat# 16600082
DMEM-F12 W Medium	Biowest	Cat# L0093-500
Fetal Bovine Serum	Gibco	Cat# 10270106
Penicilin/Streptomicin	Biowest	Cat# L0022
CTS GlutaMAX-I Supplement	Gibco	Cat# A1286001
Trypsin-EDTA (0.5%)	Gibco	Cat# 15400054
Insulin solution human	Sigma-Aldrich	Cat# I9278
Transferrin human	Sigma-Aldrich	Cat# T8158
HEPES solution	Sigma-Aldrich	Cat# H3537
ACL-4 Medium	Internal stock	N/A
HITES Medium	Internal stock	N/A
Opti-MEM I Reduced Serum Medium	Gibco	Cat# 31985047
Polybrene	Santa Cruz	Cat# sc-134220
Puromycin	InvivoGen	Cat# ant-pr-1
Dimethyl sulfoxide	Sigma-Aldrich	Cat# D2650
Harris Hematoxylin solution	Panreac Applichem	Cat# 253949
16% Formaldehyde (w/v), Methanol-free	Thermo Scientific	Cat# 28906

(*Continued on next page*)

Continued

REAGENT or RESOURCE	SOURCE	IDENTIFIER
PBS	Gibco	Cat# 20012068
Critical commercial assays		
DC Protein Assay kit	Bio-Rad	Cat# 5000111
NeoStain ABC Kit, HRP, Mouse & Rabbit, no chromogen	Quimigen	Cat# NB-23-00001–4
ImmPACT DAB Substrate kit, Peroxidase (HRP)	Vector Laboratories	Cat# SK-4105
BigDye Terminator V3.1 Cycle Sequencing kit	Applied Biosystems	Cat# 4337456
Maxwell RSC simply RNA Tissue kit	Promega	Cat# AS1340
SYBR Green PCR Master Mix	Applied Biosystems	Cat# 4309155
Halt Protease and Phosphatase Inhibitor Cocktail (100X)	Thermo Scientific	Cat# 78440
Magna ChIP Protein A + G Magnetic Beads	Sigma-Aldrich	Cat# 16–663
Deposited data		
Bulk RNA-seq data	This paper	Gene Expression Ommnibus:
Bulk RNA-seq data	(Saigi et al.[2])	Gene Expression Ommnibus: https://www.ncbi.nlm.nih.gov/geo/query/acc.cgi
Bulk RNA-seq data	(George et al.[20])	EGA European Genome-Phenome Archive: https://ega-archive.org/studies/EGAS00001000925
Bulk RNA-seq data	DepMap/CCLE	https://depmap.org/portal/download/all/
Bulk RNA-seq data	TCGA	https://doi.org/10.25504/FAIRsharing.m8wewa
ChIP-seq IRF1 data	This paper	Gene Expression Ommnibus: https://www.ncbi.nlm.nih.gov/geo/query/acc.cgi?acc=
ChIP-seq MYC data	(Llabata et al.[36])	https://www.ncbi.nlm.nih.gov/bioproject/?term=PRJNA608275
ChIP-seq MAX data	(Llabata et al.[36])	https://www.ncbi.nlm.nih.gov/bioproject/?term=PRJNA608275
ChIP-seq H3K27ac data H1299	(Romero et al.[22])	Gene Expression Ommnibus: https://www.ncbi.nlm.nih.gov/geo/query/acc.cgi
ChIP-seq H3K27ac data H23	(Handoko et al.[23])	Gene Expression Ommnibus: https://www.ncbi.nlm.nih.gov/geo/query/acc.cgi GSE113715
ChIP-seq H3K27ac data A549	ENCODE project consortium[24]	Gene Expression Ommnibus: https://www.ncbi.nlm.nih.gov/geo/query/acc.cgi?acc=GSE175131
ChIP-seq H3K27ac data H1048, DMS114, H69, H82, H128, H446	(Huang et al.[25])	Gene Expression Ommnibus: https://www.ncbi.nlm.nih.gov/geo/query/acc.cgi?acc=GSE115124
Experimental models: cell lines		
A427	ATCC	Cat# HTB-53
A549	ATCC	Cat# CRM-CCL-185
CAL-12T	DSMZ	Cat# ACC 443
CALU1	ATCC	Cat# HTB-54
CALU3	ATCC	Cat# HTB-55
DMS153	ATCC	Cat# CRL-2064
EBC1	RIKEN Cell Bank	Cat# RCB1965
H1299	ATCC	Cat# CRL-5803
H1395	ATCC	Cat# CRL-5868

(*Continued on next page*)

Continued

REAGENT or RESOURCE	SOURCE	IDENTIFIER
H1437	ATCC	Cat# CRL-5872
H1648	ATCC	Cat# CRL-5882
H1650	ATCC	Cat# CRL-5883
H2009	ATCC	Cat# CRL-5911
H2030	ATCC	Cat# CRL-5914
H209	ATCC	Cat# HTB-172
H2170	ATCC	Cat# CRL-5928
H2228	ATCC	Cat# CRL-5935
H2342	ATCC	Cat# CRL-5941
H322	ECACC	Cat# 95111734
H358	ATCC	Cat# CRL-5807
H441	ATCC	Cat# CRM-HTB-174
H596	ATCC	Cat# HTB-178
HCC15	DSMZ	Cat# ACC 496
LC-2/ad	ECACC	Cat# 94072247
LOUNH91	DSMZ	Cat# ACC 393
Lu134	RIKEN Cell Bank	Cat# RCB0466
Lu165	RIKEN Cell Bank	Cat# RCB1184
LXF289	DSMZ	Cat# ACC 265
PDC10	Pros et al.[15]	N/A
PDC13	Pros et al.[15]	N/A
PDC2	Pros et al.[15]	N/A
PDC4	Pros et al.[15]	N/A
PDC7	Pros et al.[15]	N/A
PDC8	Pros et al.[15]	N/A
PDC6	Pros et al.[15]	N/A
PDC9	Pros et al.[15]	N/A
SK-MES-1	ATCC	Cat# HTB-58
DMS114	ATCC	Cat# CRL-2066
DMS273	ECACC	Cat# 95062830
H1048	ATCC	Cat# CRL-5853
H1623	ATCC	Cat# CRL-5881
H1672	ATCC	Cat# CRL-5886
H1703	ATCC	Cat# CRL-5889
H1963	ATCC	Cat# CRL-5982
H2029	ATCC	Cat# CRL-5913
H2107	ATCC	Cat# CRL-5983_FL
H2171	ATCC	Cat# CRL-5929
H23	ATCC	Cat# CRL-5800
H345	ATCC	Cat# HTB-180
H446	ATCC	Cat# HTB-171
H460	ATCC	Cat# HTB-177
H520	ATCC	Cat# HTB-182
H522	ATCC	Cat# CRL-5810
H69	ATCC	Cat# HTB-119
H774	ATCC	Cat# CRL-5842
H82	ATCC	Cat# HTB-175
H841	ATCC	Cat# CRL-5845

(*Continued on next page*)

Continued

REAGENT or RESOURCE	SOURCE	IDENTIFIER
HCC33	DMSZ	Cat# ACC 487
LUDLU1	ECACC	Cat# 92012463
PC14	ECACC	Cat# 90071810
PDC11	Pros et al.[15]	N/A
PDC12	Pros et al.[15]	N/A
PDC14	Pros et al.[15]	N/A
H1573	ATCC	Cat# CRL-5877
H1993	ATCC	Cat# CRL-5909
H2126	ATCC	Cat# CCL-256
Oligonucleotides		
ICAM1-Forward: CACAGTCACCTATGGCAACG	Integrated DNA Technologies (IDT)	N/A
ICAM1-reverse: CCTCTGGCTTCGTCAGAATC	Integrated DNA Technologies (IDT)	N/A
IDO1-Forward: GGCAAAGGTCATGGAGATGT	Integrated DNA Technologies (IDT)	N/A
IDO1-reverse: CTGCAGTCTCCATCACGAAA	Integrated DNA Technologies (IDT)	N/A
PDCD1LG2-Forward: CCCTGGAATGCAACTTTGAC	Integrated DNA Technologies (IDT)	N/A
PDCD1LG2-reverse: TGCATTGGTACTGTCCTTCG	Integrated DNA Technologies (IDT)	N/A
SOCS1-Forward: CCCTTCTGTAGGATGGTAGCACAC	Integrated DNA Technologies (IDT)	N/A
SOCS1-reverse: GGCTCTGCTGCTGTGGAGAC	Integrated DNA Technologies (IDT)	N/A
TAP1-Forward: TGCTGAAAGTGGGAATCCTC	Integrated DNA Technologies (IDT)	N/A
TAP1-reverse: GCCCACAGCCTTCTGTACTC	Integrated DNA Technologies (IDT)	N/A
Recombinant DNA		
psPAX2 plasmid	Addgene	Cat# 12260
pMD2.G plasmid	Addgene	Cat# 12259
pEZ-LV205 plasmid	GeneCopoeia	GenBank: NM_000416.2
pLVX-IRES-ZSGreen vector	Internal stock	N/A
Software and algorithms		
Graphpad Prism 7	GraphPad Software	https://www.graphpad.com/
Gene Set Enrichment Analysis (GSEA)	Subramanian et al.[55]	https://www.gsea-msigdb.org/gsea/index.jsp
STAR (version 2.5.3a)	Dobin et al.[56]	https://github.com/alexdobin/STAR
Samtools	Li et al.[57]	http://samtools.sourceforge.net/
limma-voom	Law et al.[58]	
g: Profiler	Raudvere et al.[59]	
DESeq2 (R package, version 1.32.0)	Love et al.[60]	https://www.bioconductor.org/packages/release/bioc/html/DESeq2.html
FastQC (version 0.11.5)	Andrews et al.[61]	http://www.bioinformatics.babraham.ac.uk/projects/fastqc
skewer (version 0.2.2)	Jiang et al.[62]	
Bowtie2 (version 2.3.2a)	Langmead et al.[63]	http://bowtie-bio.sourceforge.net/bowtie2/index.shtml
MACS (version 2.1.1.20160309)	Zhang et al.[64]	https://github.com/macs3-project/MACS
HOMER's	Heinz et al.[65]	http://homer.ucsd.edu/homer/
DeepTools	Ramirez et al.[66]	https://deeptools.readthedocs.io/en/develop/
MEME-CHIP (version 5.11)	Machanick et al.[67]	
Picard method	N/A	http://broadinstitute.github.io/picard
Pheatmap (R package, version 1.0.12)	The Comprehensive R Archive Network (CRAN)	https://cran.r-project.org/web/packages/pheatmap/index.html
R version 4.2.0	The R Project for Statistical Computing	https://www.r-project.org
R studio version 0.94.102	RStudio, PBC	https://www.rstudio.com/

RESOURCE AVAILABILITY

Lead contact

Further information and requests for resources and reagents should be directed to and will be fulfilled by the lead contact, Montse Sanchez-Cespedes (mscespedes@carrerasresearch.org)

Materials availability

All unique/stable reagents generated in this study are available from the lead contact with a completed Materials Transfer Agreement.

Data availability

- All processed RNAseq and ChIP-seq data that support the findings of this study have been deposited with Gene Expression Omnibus (GEO): https://www.ncbi.nlm.nih.gov/geo/query/acc.cgi?acc=GSE186171.
- This paper does not report original code.
- Any additional information required to reanalyze the data reported in this paper is available from the lead contact upon request.

EXPERIMENTAL MODEL AND SUBJECT DETAILS

Patients

All tumor specimens were collected from patients newly diagnosed with NSCLC at the time of surgical resection or diagnostic biopsy, prior to treatment. Regarding the study of *MYC* copy number and response to ICB, patient information on gender, age and treatment line is included in Table S6. Tumor and normal matched samples were obtained from patients with appropriate consent. Procedures were approved by our Institutional Review Board (PI-19-275). Available slides were reviewed and classified according to WHO criteria.

Cancer cell lines

Cell lines were purchased from the American Type Culture Collection (Rockville, MD, USA), from the European Collection of Authenticated Cell Cultures (ECACC), the German Collection of Microorganisms and Cell Cultures (DSMZ), and the RIKEN Cell Bank (Japan). Primary cancer cells derived from malignant pleural effusions (patient-derived cancer cells, PDCs) from a previous study[15] were used. Cell lines grown under recommended conditions, supplemented with 5% fetal bovine serum and maintained at 37°C in a humidified atmosphere of 5% CO2/95% air. All cancer cell lines and PDCs were periodically tested to rule out the possibility of any contamination by *Mycoplasma* and were authenticated by testing for *TP53* and other mutations (e.g., *SMARCA4*, *STK11*, etc.) by Sanger sequencing. Genomic DNA and total mRNA were extracted by standard protocols. Whole-exome sequencing data for the PDCs was gathered from our previous publication[15] or, in the case of the commercially available LC cell lines, from public databases: CCLE (https://www.cbioportal.org/study/summary?id=ccle_broad_2019), and COSMIC-Catalogue of Somatic Mutations in Cancer (https://cancer.sanger.ac.uk/cell_lines).

METHOD DETAILS

Antibodies, western blots and immunostainings

For western blots, whole-cell lysates were collected in a buffer containing 2% SDS, 50 mM Tris-HCl (pH 7.4), 10% glycerol and protease and phosphatase inhibitor cocktail (Roche Applied Science). Protein concentrations were determined using a Bio-Rad DC Protein Assay kit (Life Science Research). Equal amounts of lysates (10 μg) were separated by SDS-PAGE and transferred to a nitrocellulose membrane that was blocked with 5% nonfat dry milk. Membranes were incubated with the primary antibody overnight at 4°C, then washed before incubation with species-appropriate IRDye 680CW (925–68022) or IRDye 800CW (925–32213) fluorescent secondary antibodies (1:10000 LI-COR, NE, USA) for 1 h at room temperature. Membranes were imaged using Odyssey Li-Cor CLx i software (Image Studio Lite v5.2).

Levels of B2M, HLA-I and PD-L1 and of CD8 T-lymphocyte intratumoral infiltration, obtained by immunohistochemistry, were available from a previous study.[8] To determine IFNGR1 levels by immunohistochemistry we used the polyclonal anti-IFNGR1 antibody (10808-1-AP, Proteintech; 1:200 dilution. Three-micrometer-thick sections from the tumors distributed in tissue microarrays were transferred to silanized glass slides. After deparaffinization and quenching with endogenous peroxidase, the slides were boiled in Tris-EDTA buffer for 30 min. After antibody incubation, immunodetection was performed with the NeoStain ABC Kit, HRP, Mouse & Rabbit, no chromogen (*Neo* Biotech) and with diaminobenzidine chromogen as the substrate (Invitrogen). Sections were counterstained with hematoxylin and evaluated under a Leica DM1000 microscope. In all the immunostainings the H596 and the PDC11 (IFNGR1-mutant) cells were include as a positive and negative control, respectively. Three investigators evaluated the sections using uniform criteria. Immunostaining in the tumor cell surface membrane was scored as follows: no staining, (−); low-intensity staining, (+); high-intensity staining, (++); and very high-intensity staining (+++). For comparative purposes, tumors with no- and low-intensity staining were considered as weak, and high- and very high-intensity tumors were considered as strong.

Construction of expression vectors and infections

The complete *IFNGR1* cDNA (NM_000416.2) was purchased from GENECOPOEIA (Rockville, MD, USA) as a stock of pEZ-Lv205 plasmids carrying a stable selection marker (Puromycin) and an eGFP sequence. A mock vector was also used as a control. The lentiviruses were generated within the 293T packaging cells. The details about the SMARCA4 constructs are available in a previous publication.[33] For IFNGR1 and SMARCA4 ectopic expression, the cells were infected with lentiviruses derived from the pLVX-IRES-ZSGreen vector and then selected by sorting GFP-positive cells, using a BD FACSAria fusion flow cytometer (Becton, Dickinson).

The (lo)MAX, (hi)MAX and (hi)MYC/MAX expression vectors were generated in a previous study.[36] Briefly, the complete MAX (NM_145112.2) and MYC (NM_002467.6) cDNAs were PCR-amplified from a retrotranscribed human RNA pool (Agilent Technologies, Santa Clara, CA, USA) using Phusion High-Fidelity DNA Polymerase (Thermo Scientific, Waltham, MA, USA), following standard protocols.

Two different sequence gene specific hairpin RNA molecules (shRNAs) for C-MYC, mRNA were designed and transduced into the H2171, H446 and H460 lung cancer cell lines. shRNA against the MSS2 yeast protein (not present in mammals) was used as scrambled (control).[68] All shRNA molecules were ligated into pLVX-shRNA2-ZsGreen plasmid from Clontech, using BamHI and EcoRI restriction enzymes.

Sanger sequencing of the *IFNGR1* gene

For mutation screening of the *IFNGR1* gene (GenBank: NM_000416.2), exons 1 to 7 and its flanking introns were amplified from 30 ng of genomic DNA. PCR products were cycle-sequenced using BigDye Terminator V3.1 Cycle Sequencing kit with DNA Analyzer 3730 (Applied Biosystems, Foster City, CA, USA). All the variants identified in the study were confirmed by the resequencing of independent PCR products. Some of the variations were also tested to determine their somatic or germline origin, using paired normal DNA.

Quantitative real-time PCRs and RNA sequencing

Total RNA was extracted using the MAXWELL RSC Simply RNA tissue (Promega). Quantitative PCR was performed in a QuantStudio5 Real-Time PCR System, using SYBR Green PCR Master Mix (Applied Biosystems, Warrington, UK). RNA was sequenced at the Spanish National Genome Analysis Center (CNAG, Barcelona, Spain), as previously described.[2] RNA-sequencing data used in this study were analyzed at the CNAG-CRG. RNA-seq reads were mapped against the human reference genome (GRCh38). The raw RNA-sequencing data produced by this study are available at GeneExpression Omnibus (GEO) under accession code GSE186171.

RNA-sequencing data were also downloaded from various databases of lung cancer cell lines and primary tumors: lung adenocarcinoma and lung squamous cell carcinomas from TCGA, PanCancer Atlas; https://portal.gdc.cancer.gov/projects; lung cancer cell lines from the Depmap/CCLE https://depmap.org/portal/download/all/; Cell_lines_annotations_20181226.txt and SCLC primaries.[20]

Gene Set Enrichment Analysis (GSEA)[55] was conducted according to the instructions (https://www.gsea-msigdb.org/gsea/index.jsp), using the indicated gene expression signatures (ranked by the n-fold values of change) as the gene sets.

Chromatin immunoprecipitation (ChIP)-sequencing of IRF1

For ChIP, cells were grown and fixed with 1% methanol-free formaldehyde (Thermo Scientific) for 10 min and quenched by 125 mmol/L glycine for 15 min at room temperature and, after that, washed twice with ice-cold PBS. The cells were then centrifuged (200 *g* at 4°C) for 5 min and the pellet resuspended in 1 mL of lysis buffer (10 mmol/L Tris-HCl, 10 mmol/L NaCl, 0.5% NP-40) containing a Halt Protease & Phosphatase Inhibitor Cocktail (Thermo Scientific; ref. 78440). The pellet was then resuspended in 1 mL of nuclear lysis buffer (1% SDS, 10 mmol/L EDTA, 50 mmol/L Tris-HCl pH 8.0, protease inhibitor) and kept at 4°C for 60 min. After another centrifugation, the lysate was sonicated with a Covaris M220 instrument to yield chromatin fragments of a size of 0.25–1.00 kb on average, then frozen at −20°C for 30 min, thawed on ice, and centrifuged at 2,500 *g*. For each ChIP reaction, 60 μL of Magna ChIP Protein A + G Magnetic Beads (Merck Millipore. Cat: #16–663) was used in accordance with the manufacturer's protocol. Before adding the sheared chromatin to the beads, Triton X-100 and Na-deoxycholate were added to a final concentration of 10% each. 1% of the chromatin volume was used for input. At least two independent ChIP experiments were performed.

Immunoprecipitated chromatin was deep-sequenced in the Genomics Unit of the Center for Genomic Regulation (CRG, Barcelona, Spain) using the Illumina HiSeq 2500 system (Illumina). Briefly, library preparation included end-repair, generation of dA overhangs, adapter ligation, size selection and removal of non-ligated adapters by agarose gene electrophoresis and amplification (18 cycles) before loading the samples into the sequencer. The data produced by this study are available at GeneExpression Omnibus (GEO) under accession code GSE186171.

Global methylation microarray analysis

Global methylation microarray data were extracted from the Sanger panel of cancer cell lines[21] to search for aberrant hypermethylation of the IFNγsign genes in 177 LC cell lines. Normalized intensities were then used to calculate DNA methylation levels (beta values). Likewise, values with low statistical power (indicated by detection values of $p > 0.01$) were excluded from the analysis.

Genotyping probes present on the chip and DNA methylation probes overlapping with known SNPs were also removed. Probes were considered to be in a promoter CpG island if they were located within a CpG island (UCSC database) and were <2,000 bp away from a transcription start site (outside chromosome X).

QUANTIFICATION AND STATISTICAL ANALYSIS

RNA sequencing data analysis

RNA sequencing and data analysis were carried out at the Spanish National Genome Analysis Center (CNAG, Barcelona, Spain), RNA-seq reads were mapped against the human reference genome (GRCh38.p13) using STAR (version 2.5.3a)[56] with ENCODE parameters. Genes were quantified using RSEM (version 1.3.0)[57] with default parameter values. A human gene annotation file was downloaded from gencode release 27 (https://www.gencodegenes.org/). Mapping and quantification quality checking were performed with "GEMTools" (https://gemtools.github.io/) and custom Python scripts. Multidimensional scaling plots were performed to inspect sample similarities using the "voom"-transformed counts. Differential gene expression was performed with "limma-voom"[58] and the function 'duplicateCorrelation' to consider patient correlation. Genes with values of FDR<5% were considered significant. Functional enrichment analysis of the differentially expressed genes was performed with g: Profiler.[59] Heatmaps showing were created with the pheatmap R package. The raw RNA-sequencing data produced by this study are available at GeneExpression Omnibus (GEO) under accession code GSE186171.

RNA-sequencing data were downloaded from different databases of lung cancer cell lines or primary tumors as indicated. FASTQ files were evaluated by FastQC (https://www.bioinformatics.babraham.ac.uk/projects/fastqc, version 0.11.5) to check sequence quality before further processing and analysis. RSEM[57] was used for transcript quantification, with the reference genome GRCh38.p13, and the resulting gene expression, as a raw count matrix, the R (version 4.0.2) package DESeq2 (version 1.28.1)[60] was used to analyze differential gene expression in each cell line. Unsupervised analyses were performed using the Ward.D2 option. Correlations were plotted using the R packages Stats (version 4.0.2) and Corrplot (version 0.90).

Gene Set Enrichment Analysis (GSEA) was conducted according to the instructions (https://www.gsea-msigdb.org/gsea/index.jsp), using the indicated gene expression signatures (ranked by the n-fold values of change and $p \leq 0.01$) as the gene sets.

Chromatin immunoprecipitation (ChIP)-sequencing data analysis

Chromatin immunoprecipitation sequencing was performed in the Genomics Unit of the Center for Genomic Regulation (CRG, Barcelona, Spain) using the Illumina HiSeq 2500 system (Illumina). For ChIP-sequencing data analysis, quality of raw reads (fastq format) was checked with FastQC (version 0.11.5).[61] Reads were trimmed using skewer (version 0.2.2)[62] and then mapped with bowtie2 (version 2.3.2)[63] to the hg38 *Homo sapiens* genome (using release 31 of Gencode annotation). Duplicated reads were removed by the Picard method "MarkDuplicates" [http://broadinstitute.github.io/picard]. Peaks were called using macs2 method[64] "callpeak" (version 2.1.1.20160309) with parameters "–extsize 300 -q 0.1 –fix-bimodal", then annotated with Homer's "annotatePeaks.pl" script. The region ±3 kb around the TSS was considered as the promoter, unless otherwise indicated. To represent the ChIP-seq signal in the heatmap and intensity plot, bedgraph files were generated using HOMER's "makeUCSCfile" function,[65] with default parameters, normalizing for differences in sample library size, and BigWig files were generated using the "bedGraphToBigWig" function from UCSC. Heatmaps were created using the functions "computeMatrix" and "plotHeatmap" in deepTools.[66]

Motif analysis was done for each cell line using MEME-CHIP (version 5.11).[67] Before motif searching, only peaks present in both biological replicates of the same cell line were considered, and 50 bp were taken on each side of peaks.

Statistical analysis

Associations between categorical variables were assessed with the chi-squared ($\chi 2$) or, if expected values were very small, Fisher's exact test. Continuous variables were summarized as means and standard deviations. Two-tailed unpaired and paired Student's tests were performed, as indicated, using Prism software. We considered any test to be significant for values of $p < 0.05$. Kaplan–Meier survival curves were compared using the log rank test. Statistical details of individual experiments are presented in the corresponding figure legends, where n indicates the number of independent biological replicates examined.